# Silver-Modified η-Al2O3 Catalyst for DME Production

Osman Ahmed, A. I., Abu-Dahrieh, J., Abdelkader, A., Hassan, N., Laffir, F., McLaren, M., & Rooney, D. (2017). Silver-Modified η-Al2O3 Catalyst for DME Production. *Journal of Physical Chemistry C*, *121*(45), 25018–25032. https://doi.org/10.1021/acs.jpcc.7b04697

**Published in:**
Journal of Physical Chemistry C

**Document Version:**
Peer reviewed version

# Silver Modified η-$Al_2O_3$ Catalyst for DME Production

Ahmed I. Osman [a,b*], Jehad K. Abu-Dahrieh[a*], Adel Abdelkader [b], Nourhan M. Hassan[a], Fathima Laffir [c], Mathew McLaren[d], David Rooney [a]

[a]School of Chemistry and Chemical Engineering, Queen's University Belfast, Belfast BT9 5AG, Northern Ireland, UK

[b]Chemistry Department, Faculty of Science - Qena, South Valley University, Qena 83523 – Egypt

[c] Bernal Institute, University of Limerick, Limerick, V94 T9PX, Ireland

[d]Centre for Nanostructured Media, School of Mathematics and Physics, Queen's University Belfast, BT7 1NN, UK.

* Corresponding author

*Jehad K. Abu-Dahrieh, Ahmed I. Osman*

E-mail: j.abudahrieh@qub.ac.uk, aosmanahmed01@qub.ac.uk

Address: School of Chemistry and Chemical Engineering, Queen's University Belfast, David Keir Building, Stranmillis Road, Belfast BT9 5AG, Northern Ireland, United Kingdom

Fax: +44 2890 97 4687

Tel.: +44 2890 97 4269

**Abstract**

Herein, an in-situ DRIFT technique was used to study the reaction mechanism of methanol dehydration to dimethyl ether (DME). Moreover, the effect of silver loading on the catalytic performance of η-$Al_2O_3$ was examined in a fixed bed reactor under the reaction conditions where the temperature ranged from 180-300 °C with a WHSV= 48.4 $h^{-1}$. It was observed that the optimum Ag loading was found to be 10% Ag/η-$Al_2O_3$ with this novel catalyst also showing a high degree of stability under steady-state conditions and this is attributed to the enhancement in both the surface Lewis acidity and hydrophobicity.

## 1. Introduction

Air pollution and global warming due to the combustion of carbon-based non-renewable resources for transportation are two major global challenges. The production of clean biofuel such as dimethyl ether (DME) is an attractive alternative for pollution mitigation. DME is an environmentally friendly fuel with clean-burning and smoke-free emissions[1]. The attractive combustion properties are due to it is containing neither sulphur nor nitrogen which leads to the absence of $SO_x$ emissions and the possibility of the absence of NOx emissions at low combustion temperatures. Usually, at high combustion temperatures, the release of NOx emissions comes from nitrogen and oxygen of the air. The lack of direct carbon-to-carbon bonds means it does not generate particulate matter (PM) emissions. DME can be produced by two main routes; either from syngas using a bi-functional catalyst (Equation 1) or via the dehydration of methanol over solid catalysts such as $Al_2O_3$ (Equation 2), according to the following reactions [1-5]:-

$$3CO + 3H_2 \leftrightarrow CH_3OCH_3 + CO_2 \quad (1)$$

$$2CH_3OH \leftrightarrow CH_3OCH_3 + H_2O \quad (2)$$

The synthesis of efficient and commercially attractive, robust catalysts has become increasingly challenging due to the both increased demand for DME production and the catalytic process required for methanol to DME process (MTD). Alumina is a cost-efficient material that can be tailored to unique textural properties including high surface area and high porosity. Therefore, optimizing $Al_2O_3$ as a catalyst for this process remains a topic of great importance [6]. Extensive studies were performed on γ-$Al_2O_3$ for MTD reaction, however, in our previous publication [7]; we showed that η-$Al_2O_3$ catalyst is more active than that of γ-$Al_2O_3$. Few publications have studied the mechanism and the kinetic modelling of η-$Al_2O_3$ in MTD reaction, therefore, this area requires further examination.

The dehydration reaction occurs over a solid acid catalyst where its acidity plays a big role in product distribution. Over very strong acidic sites, further dehydration will take place producing olefins. In order to suppress the dehydration to olefins reaction and increase the selectivity towards the DME, weak or moderate acidity catalysts are desirable as in the $Al_2O_3$. Methanol dehydration is known to take place on

Lewis acid-pair sites and its rate increases as the surface Lewis acidity increases [8]. It was well reported that γ-$Al_2O_3$, a typical Lewis acid catalyst and also the η-$Al_2O_3$ used in the study, can catalyse dehydration of methanol to DME [7]. Several reaction mechanisms have been presented for methanol dehydration on acid catalysts [8-9]. Either Brønsted acid sites or Lewis acid-base pair sites are believed to play a role in such reaction and, generally, the stronger the acid sites the more active the catalysts, however, it should be remembered that as far as Brønsted sites are concerned, their strength and the reaction temperature should be controlled to avoid hydrocarbons formations [7]. The mechanism based on the Lewis acidity, on the other hand, requires adjacent acid-base pair sites to provide the reaction between the adsorbed alcohol molecule on an acidic site and an adsorbed alkoxide anion on a basic site [8].

The most widely used catalyst for the MTD reaction is $Al_2O_3$ however; modifications are needed to increase the weak acidity of alumina along with the water deactivation due to its superhydrophilic properties. To enhance the acidity, group 11 elements such as Cu, Ag and Au were used to improve the Lewis acidity as they act as electron acceptors. In a recent study by Camposeco et al.[10], they studied the effect of Ag loading on the acidity of titania nanotubes by using FTIR analysis of adsorbed pyridine on the support. They found that after Ag loading, the Lewis acidic sites on the $TiO_2$ support increased. Gora-Marek et al. [11] also reported an increase in the Lewis acidity of different supports with Ag loadings and reported that silver cations act as strong electron acceptors which can also be considered as Lewis acids. Furthermore, they used the same catalyst (Ag/$Al_2O_3$) for selective ammonia oxidation and mentioned that the high catalytic performance of 10 wt. % Ag/$Al_2O_3$ was related to the specific interaction between the Ag and alumina support along with the high Ag dispersion over the surface of the alumina support.

Furthermore, in the MTD process water is produced which also has a significant effect on catalyst deactivation [12-15] as $Al_2O_3$ is super-hydrophilic [16], and facilitates strong water adsorption. Both water and methanol compete for adsorbing on the active sites of $Al_2O_3$ with water being adsorbed more strongly [12]. It is possible to increase the hydrophobicity of the support thereby reducing the deactivation by water. Several techniques can be employed for this purpose; for instance, Zhao et al. [17] used the electrodeposition

of silver aggregate to prepare superhydrophobic surfaces with water contact angle (CA) of 154º. An electroless galvanic deposition method was used by Feng et al.[18] to fabricate superhydrophobic Ag nano-coatings with a CA of 156.4º, where the coatings showed a high thermal stability; the CA did not change with heating up to 200 ºC for 2hrs. Li et al.[19] prepared a superhydrophobic coating of silver-doped titania @ polycarbonate with a CA >160º. Wu et al.[20] demonstrated a convenient solution dipping method to make self-healing superhydrophobic materials using Ag nanoparticles that prepared from silver nitrate solution with a CA of 159 º. Recently, copper was used to prevent the strong binding of $H_2O$-$Al_2O_3$ by enhancing the surface hydrophobicity with CA =12º for 6% $Cu/Al_2O_3$ catalyst that was used for the MTD reaction[21]. Jo et al.[22] reported that the addition of Si to η-$Al_2O_3$ by using TEOS (tetraethyl orthosilicate) enhanced the MTD conversion.

$Ag/Al_2O_3$ catalyst is commonly used in the catalytic reduction of $NO_x$ reaction [23-27]. To the extent of the authors' knowledge, no research has been done using that catalyst in the methanol dehydration reaction to produce DME. The above discussion highlights the necessity of understanding the mechanism of MTD over η-$Al_2O_3$ catalyst along with the kinetic modelling study. Furthermore, the modifications of η-$Al_2O_3$ catalyst in term of the acid site strength and water deactivation need to be studied more closely. This suggests that the addition of a metal onto the support could modify the properties of the catalyst surface, for instance, the addition of silver to the alumina surface could decrease the water adsorption by changing the hydrophobicity of the surface, leading to an increase in activity. However, high Ag loadings could partially block the pore volume of the alumina support. The balance between these two effects suggests that an optimum loading exists where it is recognised that this will likely be a function of the original support. Herein, we studied the mechanism of the MTD reaction using the DRIFTS (Diffuse Reflectance Infrared Fourier Transform) technique along with the kinetic modelling. Moreover, we investigated the potential benefits of loading of Ag onto η-$Al_2O_3$ for the production of DME via the MTD reaction in term of dispersion, acidity and hydrophobicity.

## 2. Experimental

### *2.1 Materials and methods*

The chemicals used in the present study were all of analytical grade and supplied by Aldrich, UK. The chemicals included aluminium nitrate nonahydrate [$Al(NO_3)_3 \cdot 9H_2O$], silver nitrate ($AgNO_3$, >99%), Triethoxy(octyl)silane (TEOOS, ≥97.5%) and ammonia solution (35%). The commercial γ-$Al_2O_3$ (BET = 117 $m^2/g$, pore size=1.035 nm) was prepared by crushing γ-$Al_2O_3$ pellets (Alfa Aesar). The He, $H_2$ and air gases were purchased from BOC with purity 99.99%.

### *2.2 Catalyst preparation*

#### *2.2.1 Pure catalyst:*

The preparation of alumina supports has been described elsewhere [7]. It was prepared from aluminium nitrate nonahydrate that was then precipitated by ammonia solution, the resulting precipitate was calcined at 550 °C and designated as η-$Al_2O_3$.

#### *2.2.1 Hydrophobic catalyst:*

The preparation of the hydrophobic alumina was carried out using triethoxy(octyl)silane (TEOOS). Firstly, 5g of the η-$Al_2O_3$ catalyst was sonicated in 100 mL of toluene for 1 hr, afterwards, 3 mL of TEOOS was added then the whole solution was refluxed for 3hrs. Subsequently, a centrifugation at 4500 rpm was performed to recover the precipitated powder, followed by washing several times with toluene to remove the un-reacted TEOOS. Finally, the resulted powder was dried overnight at 120 ºC and designated as H-$Al_2O_3$.

#### *2.2.3 Silver metal loadings on* η-$Al_2O_3$:

Silver loaded catalysts were prepared by wet impregnation with the aid of sonication. Pure η-$Al_2O_3$ was loaded with x% (wt/wt) of silver (where x= 1, 10 or 15%). Calculated amounts of silver nitrate were

dissolved and/or dispersed with a known amount of support, in ~ 5 mL deionized water. This was sonicated at 80 °C (Crest ultrasonic bath model 200 HT), at a frequency of 45 kHz, resulting in a homogeneous paste. All mixtures were then evaporated to dryness. Herein, catalysts loaded with 1, 10, and 15% which were then calcined 550 °C are denoted as follows: *X*%Ag/η-$Al_2O_3$ where *X* is the weight percentage of Ag.

*2.3 Catalyst Characterization*

In-situ DRIFTS study of methanol dehydration over pure η-$Al_2O_3$ sample was performed during a temperature ramp from 50 to 250°C under reaction feed. The DRIFTS study was performed in order to investigate the adsorption/desorption properties of the catalyst surface towards methanol dehydration and to elucidate some aspects of the reaction mechanism over this catalyst, using a Bruker Vertex 70 FTIR Spectrometer equipped with a liquid $N_2$ cooled detector. Before exposure to the reaction feed, the pre-treated catalyst surface was taken as the reference and was subtracted as the spectra's background.

Powder X-ray diffraction (XRD) analyses of the catalysts were carried out using a PANalytical X'Pert Pro X-ray diffractometer. This diffractometer was equipped with a CuKα X-ray source with a wavelength of 1.5405 Å. Diffractograms were collected from 15° to 80°. The X-ray tube was set at 40 kV and 40 mA. Once the scan had finished, the main peaks were selected and compared to diffraction patterns from the software library. The pattern with the highest percentage match was used. The particle size was calculated according to the Scherrer equation.

Brunauer-Emmett-Teller (BET) analysis was performed using a Micromeritics ASAP 2010 system. The BET surface areas and pore volumes were measured by $N_2$ adsorption and the desorption isotherms at liquid nitrogen temperature (-196 °C).

TPD-pyridine was used to determine the total surface acidity of the catalyst using the adsorption of pyridine as a probe molecule. Small portions (50 mg) of each sample were pre-heated to 250 °C for 2 hrs in air before exposure to the probe molecule (pyridine) in a sealed desiccator for two weeks. The pyridine–covered samples were subjected to Thermogravimetric (TG) analysis on heating up to 600 °C at heating

rate of 20 °C.min$^{-1}$ in dry $N_2$ (flow rate = 40 ml.min$^{-1}$). The weight loss due to desorption of pyridine from the acidic sites was determined as a function of total surface acidity as sites.$g_{cat}^{-1}$ [7].

Temperature-programmed reduction (TPR) was used to investigate the reducibility of the catalysts using a Micromeritics Autochem 2910 apparatus with the $H_2$ uptake monitored by a TCD. The catalyst sample (0.1 g) was placed in a quartz tube and Ar flowed over it until the temperature decreased to 30 °C. 5% $H_2$/Ar with a flow rate 30 mL min$^{-1}$ was then passed over the catalyst until a stable baseline was obtained after which the sample was heated at 10 °C min$^{-1}$ up to 700 °C.

XPS was performed in a Kratos AXIS ULTRA spectrometer using monochromatic Al Kα radiation of energy 1486.6 eV. High-resolution spectra of Ag *3d,* O *1s* and Ag MNN were taken at a fixed pass energy of 20 eV, 0.05 eV step size and 100 ms dwell time per step. Surface charge was efficiently neutralized by flooding the sample surface with low energy electrons. Core level binding energies were corrected using C *1s* peak at 284.8 eV as charge reference. For construction and fitting of synthetic peaks of high-resolution spectra, mixed Gaussian-Lorenzian functions with a Shirley type background subtraction were used.

The relative strength of the Lewis acid sites was determined by DRIFT analysis of adsorbed pyridine using a Bruker Vertex 70 FTIR Spectrometer equipped with a detector cooled with liquid $N_2$. Prior to these measurements, samples were pre-treated by outgassing at 120 °C for 0.5 h under an Ar atmosphere. Subsequently, the samples were saturated with pyridine at 50 °C then the physisorbed pyridine was removed by flushing at ~25 °C with Ar gas for 0.5 h. Fresh samples (catalyst without pyridine) were used to record the IR background under Ar flow at 300 °C. Then, the pyridine (Py) adsorbed samples were placed in the DRIFT cell at 40 °C. The samples were heated under Ar at a flow rate of 50 cm$^3$/min and the *in situ* DRIFT spectra were recorded at a resolution of 4 cm$^{-1}$ and with an accumulation of 56 scans every 30 s. The spectra after pyridine desorption were subtracted from those measured before pyridine adsorption (fresh samples) to observe the bands corresponding to Lewis and Brönsted acidic sites.

The static contact angle of the catalyst pellets with water was measured using a contact angle meter equipped with a CCD camera (FTA1000 Drop Shape Instrument- B Frame system). The morphology of the catalysts' surface was characterized by transmission electron microscopy (TEM) using a FEI Tecnai F20 at 200 kV using bright field TEM, selected area electron diffraction (SAED) and high angle annular dark field (HAADF) scanning TEM (STEM).

Scanning electron microscope (SEM) images were obtained on a FEI Quanta 250 FEG MKII with a high-resolution environmental microscope (ESEM) using XT microscope Control software.

*2.4 Catalyst activity*

Catalyst activity tests were conducted in an isothermal fixed-bed reactor made of stainless steel (6 mm OD). The catalyst bed consisted of 50-200 mg (250-425 μm) of a catalyst placed between two plugs of quartz wool. Aera mass flow controllers were used to control the flow of gases to the reactor. The liquid methanol was injected *via* a Cheminert® M Series liquid handling pump. A stable flow of methanol vapour to the reactor was established by passing the combined flow of He and methanol through a saturator system, with the evaporation chamber maintained at 150 °C. To prevent condensation, all lines were heated to ~ 150 °C. This mixture was then fed to the fixed bed reactor. The reaction conditions used were different % MeOH in the kinetic experiments and 20% MeOH in the Ag/η-$Al_2O_3$ experiments under atmospheric pressure over a temperature range from 180 to 300 °C. The total flow rate was 100 $cm^3.min^{-1}$. Before the reaction, the catalyst was activated in a stream of pure He at 325 °C for 3 h under atmospheric pressure. Then, the methanol and He mixture were fed to the reactor and samples analysed by on-line gas chromatography (Perkin-Elmer 500) equipped with a TCD and a Flame Ionisation Detector (FID). A Hayesep DB column was used for the separation of CO, $CO_2$, DME, MeOH, $CH_4$, $C_2H_4$, $C_2H_6$, ethanol, propanol, and butanol. Each data point was repeated 5 times to determine the reproducibility of the data for the products

As shown in Eq. 3, the methanol conversion ($X_{MeOH}$) was calculated on the basis of the molar flow rate of methanol in the feed ($F_{MeOH,\,in}$) and in the outlet stream ($F_{MeOH,\,out}$):

$$X_{MeOH} = \frac{F_{MeOH,in} - F_{MeOH,out}}{F_{MeOH,in}} \quad (3)$$

DME formation rate ($r_{DME}$) was determined using Eq. 4, which represents the actual moles of the produced DME per unit time ($F_{DME,actual}$) per gram of the catalyst:

$$r_{DME} = \frac{F_{DME,actual}}{wt.\,of\ the\ catalyst} \times 100\% \quad (4)$$

The selectivity for DME ($S_{DME}$) was determined using Eq. 5 as the ratio (expressed in mole%) between the content of carbon in the product DME and the sum of carbon content corresponding to all observed organic products which are present in the reactor outlet stream:

$$S_{DME} = \frac{2F_{DME}}{F_{CO2} + F_{CO} + 2F_{DME} + \sum_i n_{Ci}F_i} \times 100\% \quad (5)$$

Here, $F_{DME}$, $F_{CO2}$ and $F_{CO}$ are the molar flow rates of DME, $CO_2$ and CO respectively in the outlet stream, $n_{Ci}$ is the number of carbon atoms for each of the hydrocarbons (byproducts) and $F_i$ is the molar flow rate of these hydrocarbons [28].

## 3. Results and Discussion

### *3.1 Mechanism study of pure alumina using DRIFTS technique:*

Figure 1 shows the DRIFT spectra of η-$Al_2O_3$ sample obtained during the exposure to the reaction feed with a stepwise increase in the reaction temperature. The spectrum obtained at 50°C is characterised by negative bands in the (3800–3500 $cm^{-1}$) region and bands at 3260, 2943, 2870, 2830, 2600, 2070 and 1450 $cm^{-1}$. The negative bands (i.e. 3763 and 3740 $cm^{-1}$) are attributed to the loss of hydroxyl groups initially present on the $Al_2O_3$ surface due to the formation of hydrogen bond between surface hydroxyl groups and the adsorbed methoxy species [9, 29]. The broad peak around 3260 $cm^{-1}$ is attributed to the stretching mode of these hydrogen-bonded hydroxyl groups [9, 29]. The bands located at 2943, 2870 and 2830 can be attributed to the symmetric ν(CH3) stretching mode of adsorbed methoxy groups produced due to the dissociative adsorption of methanol on the η-$Al_2O_3$ catalyst surface [9, 29-31]. The band at 2600

$cm^{-1}$ can be assigned to a combination band of two different modes (methyl rock and methyl deformation) of the adsorbed methoxy species [9, 29-31]. The band at 2070 is likely due to adsorbed CO which may form as a result of the decomposition of formate species while the band at 1450 $cm^{-1}$ can be attributed to carbonate–carboxylate species [29, 32-33]. The formation of CO and carbonate–carboxylate species can be correlated to the occurrence of side reactions that are not involved in the dehydration reaction of methanol [9]. The stepwise increase in the temperature of the reaction feed results in a progressive decrease in the intensity of the bands at 3260, 2600, 2070 and 1450 $cm^{-1}$. A progressive decrease in the intensity of the surface hydroxyl negative bands is observed by increasing the temperature which indicates a partial restoration of hydroxyl groups on the alumina surface [9, 29]. This is due to the desorption of some of the adsorbed methoxy species that form hydrogen bonds with these hydroxyl groups which is confirmed by the accompanying decrease in the intensity of the bands at 3260 and 2600 $cm^{-1}$.In addition, bands at 1599, 1390 and 1375 $cm^{-1}$ corresponding to surface formate species started to appear at 200°C and became more intense by increasing the temperature up to 250°C [9, 29, 33-34]. Apart from the observed decrease in the intensity of some bands and the increase in the intensity of the others, there is no notable change in the band positions can be observed as temperature increases.

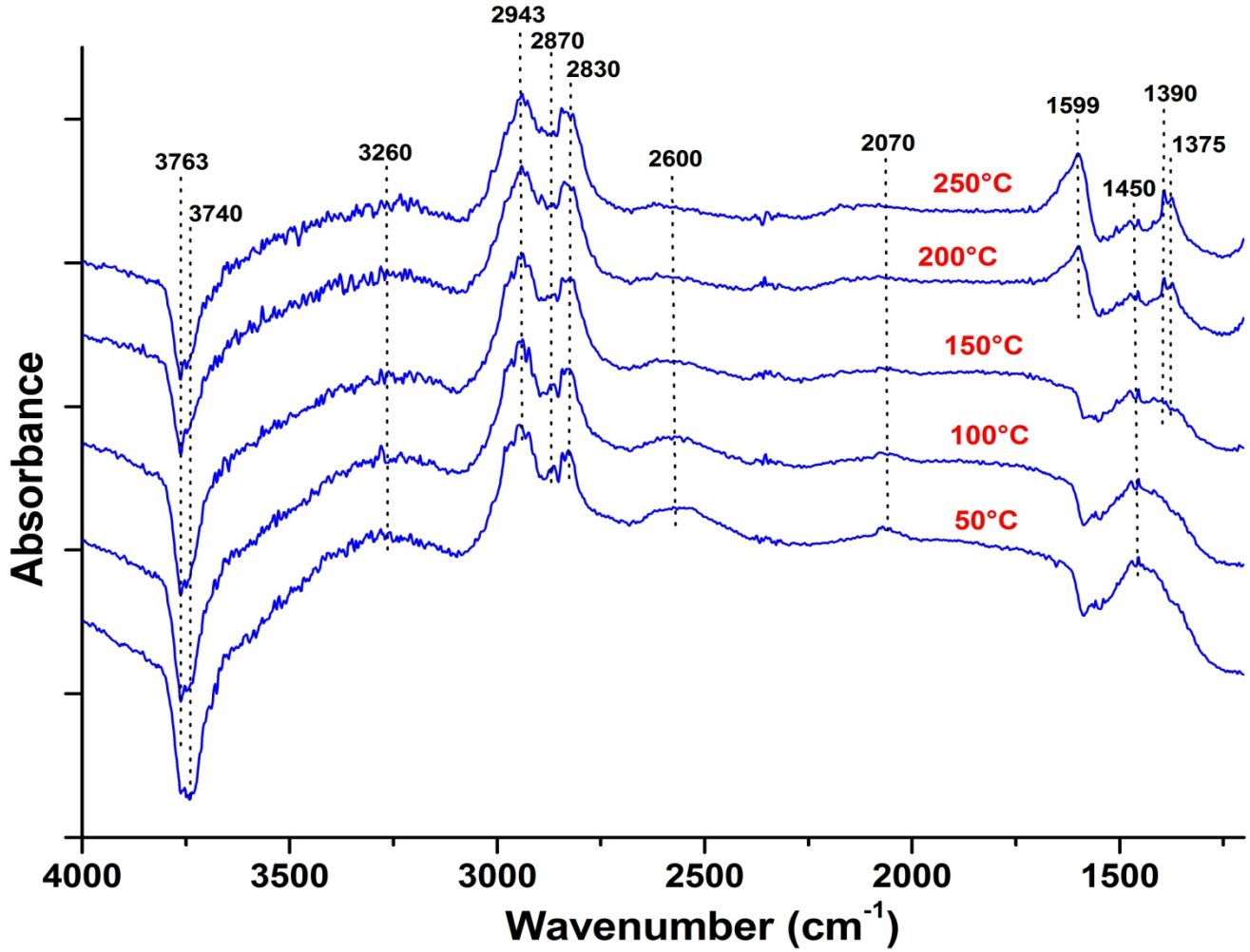


**Figure 1:** In-situ DRIFT spectra obtained over the pure η-$Al_2O_3$ catalyst during the interaction under reaction feed (20% MeOH+ He gas as an inert in the feed) at 50°C for 20 min followed by a stepwise heating to the indicated temperatures under the same reaction feed.

The mechanism of MTD over alumina catalysts may take place by two possible routes [9]: In the first route, the adsorbed methoxy species interacts with un-dissociated or molecularly adsorbed methanol, while in the second route, the reaction takes place between two adsorbed methoxy species. In the present study, the DME production started at temperatures higher than ~ 200°C, which supports the second route, as only methoxy species and not un-dissociated methanol are present on the catalyst surface at this temperature or at higher temperatures.

### *4. Silver modification* η-$Al_2O_3$

*4.1 Catalyst characterisation*

The XRD patterns of η-$Al_2O_3$ catalyst along with silver modifications at different levels of loadings (1, 10 and 15 wt. % Ag) are shown in Figure 2. The diffraction lines corresponding to the η-$Al_2O_3$ phase decreased with increasing the Ag loading, due to the metal coverage onto the η-$Al_2O_3$ support with increasing the silver metal loadings which is in agreement with the work done by Yuan et al. [35]. The catalyst 15% Ag/ η-$Al_2O_3$ with the highest Ag loading showed diffraction lines related to hexagonal $Ag_2O$ (100) at 2θ= 33.6 and 38.39 (JCPDS no. 72-2108) and minor diffraction line for the metallic silver at 2θ= 77.30 Å (ICDD 76-1393) [36]. It is worth noting that all catalysts showed amorphous structures with broad diffraction peaks.

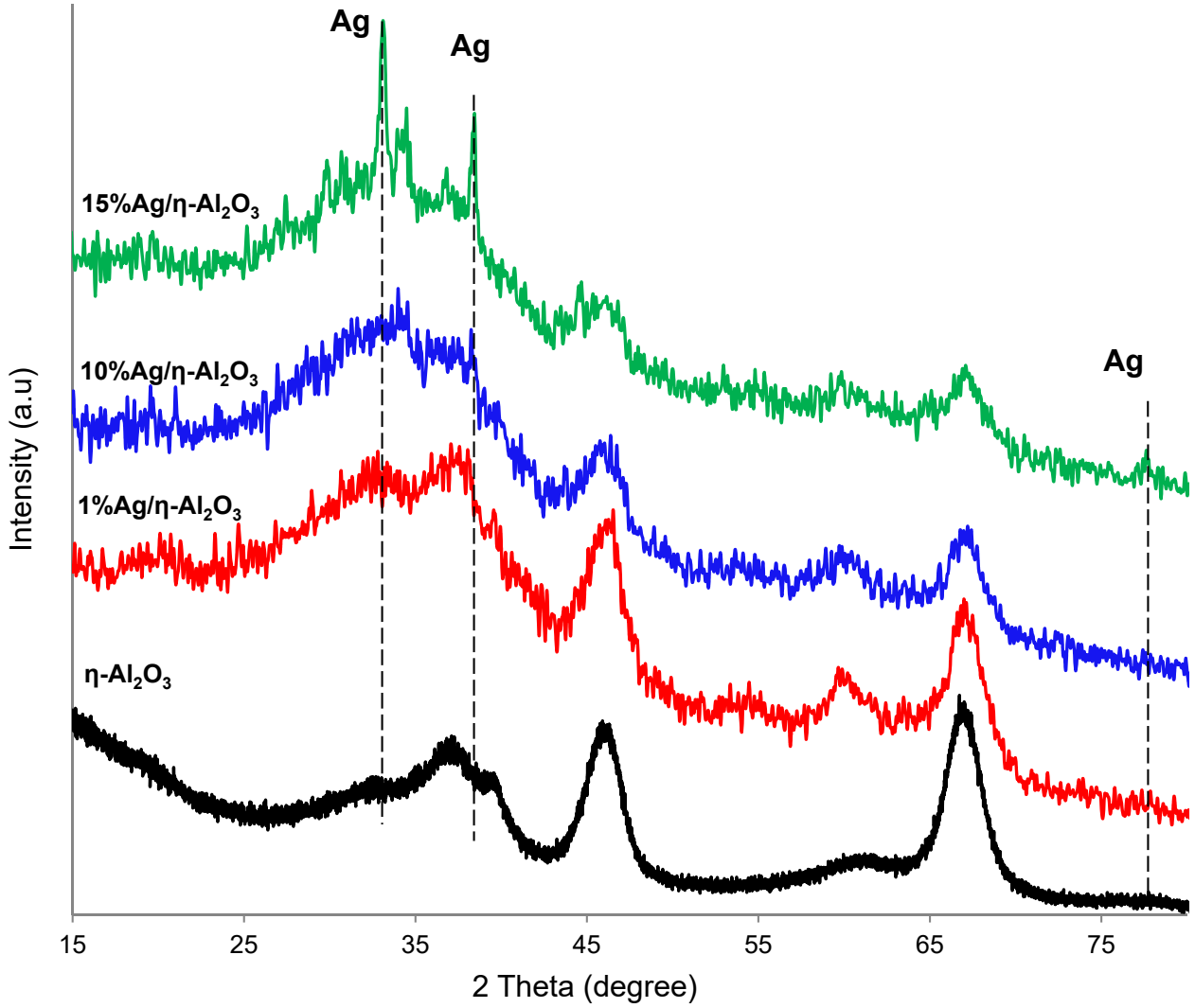


**Figure 2:** XRD patterns of η-$Al_2O_3$ catalyst along with silver modifications at different levels of loadings (1, 10 and 15 wt. % Ag).

**Table 1**: Surface area, pore volume, total acidity and acid density along with the EDX results of pure and Ag modified η-$Al_2O_3$ catalyst.

| Support / Catalyst | $S_{BET}$ ($m^2$ $g^{-1}$) | Cryst. size (nm) | Pore volume ($cm^3$ $g^{-1}$) | Total acidity[a], A(sites/g) | Acid density[b], B(sites/$m^2$) | EDX results | | | XPS results | |
|---|---|---|---|---|---|---|---|---|---|---|
| | | | | | | Al | O | Ag | IAg/IAl | %C |
| **η-$Al_2O_3$** | 223 | 5.5 | 0.5 | 8.56 | 3.8 | 51.9 | 48.1 | -- | -- | |
| **1% Ag/η-$Al_2O_3$** | 222 | 3.1 | 0.33 | 8.76 | 3.95 | 43.5 | 55.5 | 1 | 0.01 | 10.2 |
| **10% Ag/η-$Al_2O_3$** | 218 | 3.8 | 0.27 | 9.80 | 4.5 | 32.5 | 57.5 | 10 | 0.07 | 13.7 |
| **15% Ag/η-$Al_2O_3$** | 202 | 4.2 | 0.26 | 9.82 | 4.8 | 33.3 | 51.0 | 15.7 | 0.11 | 14.5 |

[a] Total acidity = A x $10^{20}$, measured by TPD-Pyridine.

[b] Acid density = B x $10^{18}$, , measured by TPD-Pyridine.

The Nitrogen adsorption-desorption isotherms of silver modified catalysts with different loadings (1, 10 and 15 wt. % Ag) on η-$Al_2O_3$ acidic support catalyst showed type IV isotherm of mesoporous structures implying a mesoporous structure. It is obvious that there is a slightly small difference in the pore volume after loading the Ag, where the pore volume decreased from 0.33 to 0.26 $cm^3/g$ at % loading of 1 and 15% Ag, respectively as seen in Figure S1. Furthermore, the surface area also declined from 222 to 202 at the same metal loadings as seen in Table 1. It is obvious that the total surface acidity and the acid density are increasing with increasing the Ag loadings.

The surface structure of the modified catalyst using the scanning electron microscope with both BSED (Back-Scattered Electrons Detector) and ETD detectors (Everhart-Thornley Detector) are shown in Figures 3 and S2, respectively. Elements of higher atomic number appear brighter in the image due to a large number of back-scattered electrons (BSE) [37]. It is apparent from Figure 3 that images of 15% Ag/η-$Al_2O_3$ catalyst appeared with far more lighter spots than that of 1% Ag/η-$Al_2O_3$ catalyst. Catalyst 10% Ag/η-$Al_2O_3$ showed good pellet particle size distribution where at low loading (1 wt. %) Ag is hardly distinguished over the surface of the catalyst and at the highest loading (15 wt. %) Ag formed a separated island with big clusters that can be confirmed using the ETD detector as seen in Figure S3. However, the orientation of particles towards the detector plays also a significant role. So, image interpretation based on brightness is arbitrary unless it is a flat sample.

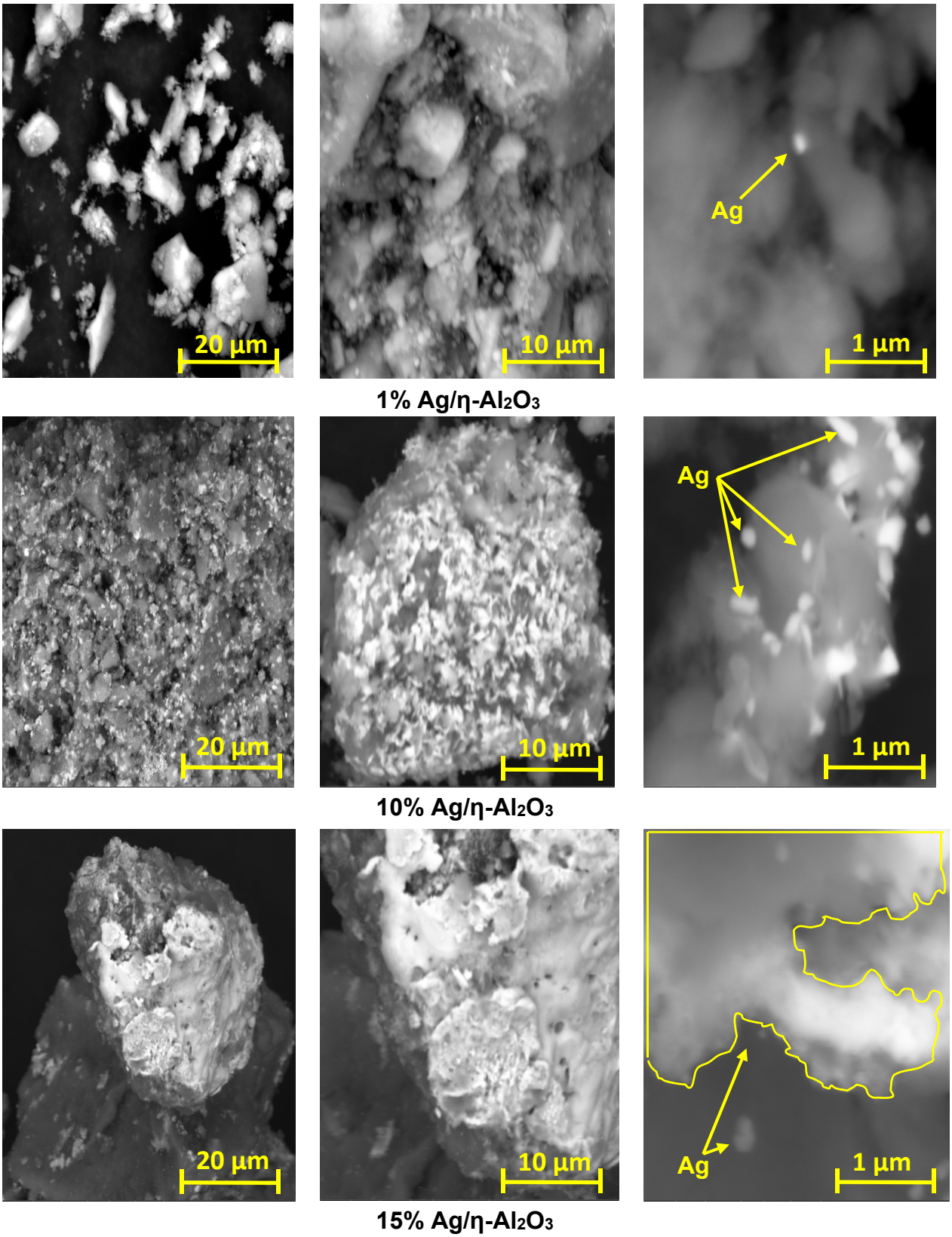


**Figure 3:** SEM images of 1% Ag/η-$Al_2O_3$, 10% Ag/η-$Al_2O_3$ and 15% Ag/η-$Al_2O_3$ catalysts at a different level of magnifications using the BSED detector where the Ag element is shown as bright areas on the image.

The EDX maps for the modified catalyst are shown in Figure 4. It is not surprising that catalyst 1% Ag/η-$Al_2O_3$ showing the fewest spots of Ag over the surface of the catalyst. While 10% Ag/η-$Al_2O_3$ catalyst showed good pellet particle size distribution among the series of the prepared catalysts. Further loading of Ag, 15% Ag/η-$Al_2O_3$, apparently high concentration of Ag spots appeared with an isolated island formation along with darker spots i.e. less existence of alumina is observed over the Al maps as seen in Figure 4.

The elemental surface composition of the modified catalysts is shown in Figure S3 and Table 1. It is obvious that the wt. % of Ag increased with increasing the Ag loading with 1, 10 and 15.7 wt. % for 1% Ag/η-$Al_2O_3$, 10% Ag/η-$Al_2O_3$ and 15% Ag/η-$Al_2O_3$, respectively. On the other hand, the wt. % of Al decreased from 43% to around 33% with increasing the Ag loading from 1 to 15 wt. %, respectively.

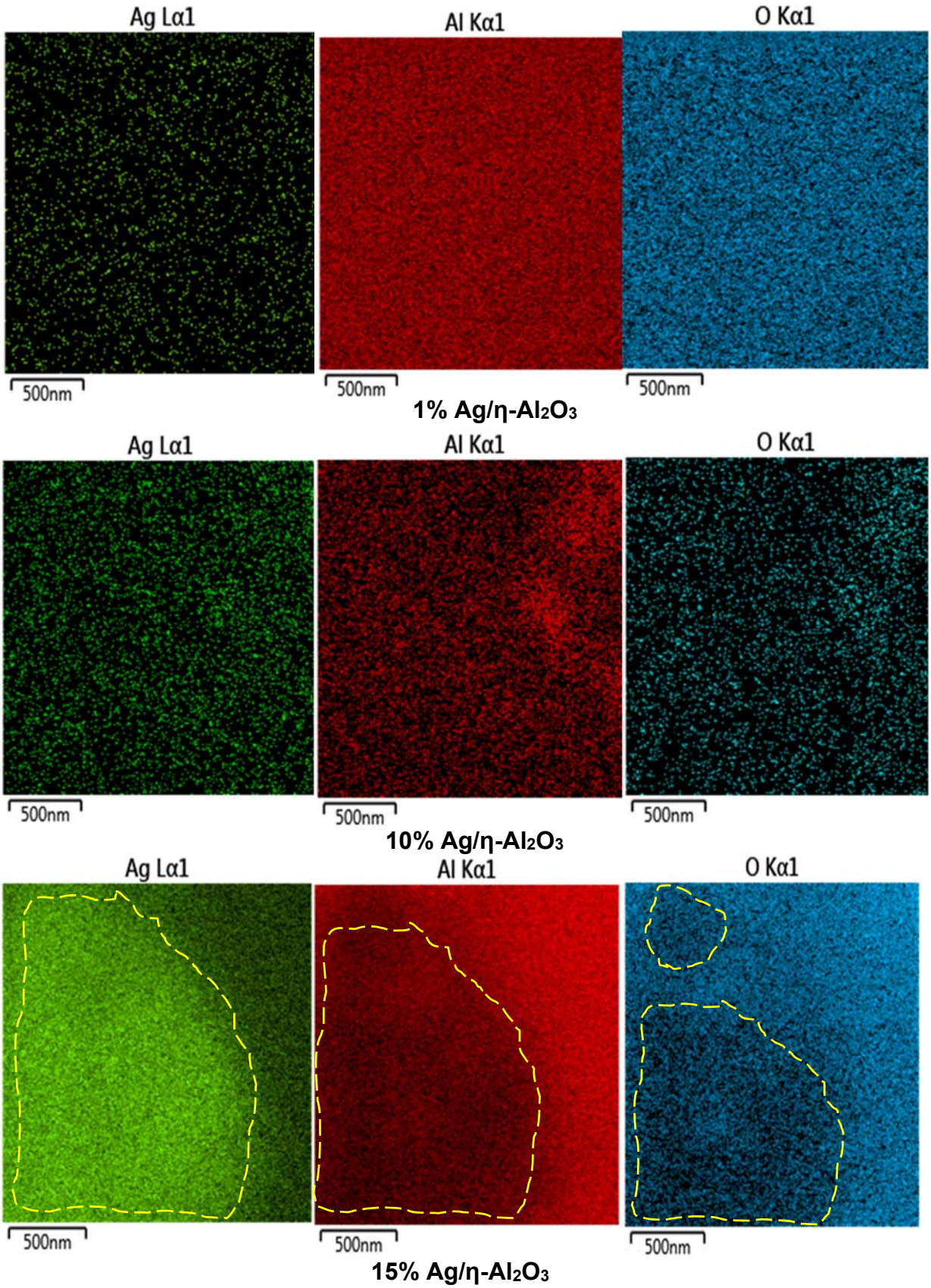


**Figure 4:** EDX maps of 1% Ag/η-$Al_2O_3$, 10% Ag/η-$Al_2O_3$ and 15% Ag/η-$Al_2O_3$ catalysts at the same level of magnification using the ETD detector.

The surface acidity of the pure and the modified catalysts were characterised using *in-situ* DRIFT-pyridine analysis as shown in Figure 5. The pure η-$Al_2O_3$ catalyst showed mainly Lewis acidic sites and the modified catalysts followed the same trend. The adsorption bands of pyridine at 1600 and 1445 $cm^{-1}$ are ascribed to strong Lewis acidic sites while the band at 1582 $cm^{-1}$ attributed to pyridine adsorbed on weak Lewis acidic sites. The adsorption band at 1482 $cm^{-1}$ is attributed to pyridine adsorbed on both Lewis and Brönsted acid sites [7]. The band intensities of pyridine on all sites were greater on the modified silver alumina catalysts showing a greater number of Lewis acidic sites than pure η-$Al_2O_3$. Apparently, the adsorption bands slightly increased with 1wt. % Ag loading, with a significant increase of Lewis acidic sites in 10% Ag/ η-$Al_2O_3$ catalyst. These results in agreement with Camposeco et al.[10] who investigated the surface acidity of Ag modified titania catalyst and showed that silver increases the Lewis acidic sites by forming $Ag^{1+}$ ions on the surface of alumina catalyst. Silver increased the acidity of the pure support which may be attributed to the electronegativity. By adding more electron deficient element (Ag) with an electronegativity of 1.93 compared to the Al metal in the pure η-$Al_2O_3$ catalyst with an electronegativity of 1.61, then Ag will act as an electron acceptor due to its higher electronegativity. This hypothesis is in agreement with the work done by Gora-Marek et al. [11] who reported an increase in the Lewis acidity of the supports with Ag loadings and reported that silver cations act as strong electron acceptors (higher electronegativity) which can also be considered as Lewis acids. The presence of $Ag_2O$ species as confirmed by the XPS and XRD analyses along with the minor contribution of Ag(0) increased the Lewis acidity, so in this case, the number and the strength of the acidic sites should be different from those of the pure η-$Al_2O_3$. The pyridine adsorption on Ag species was not excluded during the analysis.

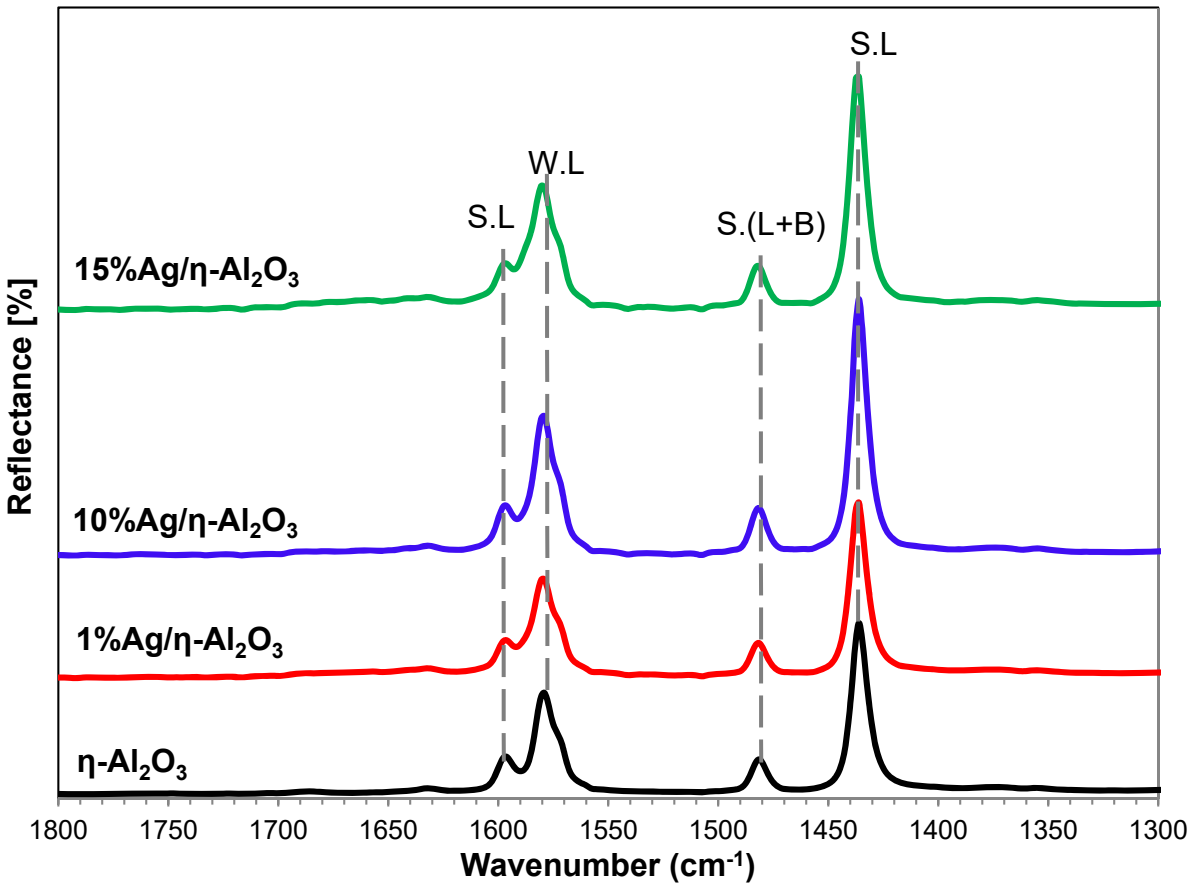


**Figure 5:** In-situ DRIFT spectra of pyridine adsorbed on the modified η-$Al_2O_3$ catalysts prepared from different loading of silver metal along with the pure η-$Al_2O_3$ catalyst.

XPS was performed to analyse the surface chemistry of the pure and Ag modified catalysts. High-resolution spectra of Ag *3d* and O *1s* (531.5 eV) along with the adventitious carbon (*C 1s*) are shown in Figure 6 [38]. The principle Ag $3d_{5/2}$ peak at approx. 368.2 eV is broad and symmetric; and energy loss features related to metallic silver is not observed on the higher binding energy side of the peak and therefore it is suggestive of the presence of $Ag_2O$. As expected, the relative intensity of silver increases with increasing Ag loading. The O*1s* characteristic of η-$Al_2O_3$ shifts to lower binding energy with increasing silver loading. Silver oxide appears at lower O *1s* binding energy and as the silver loading increases, the contribution from the silver oxide shifts the oxygen peak to lower binding energies i.e. the Ag loading facile the oxidation cycle. [39]. Since the modified catalysts were left in the air, the *C 1s* spectra showed component peaks corresponding to adsorbed carbonaceous species (CO, $CO_2$ and $CO_3$) and with adventitious carbon C-C at 284.8 eV, adsorbed CO at 286.2 eV and O-C=O at ~288.6 eV (Figure 6 (c)) [40]

with 15% Ag/η-$Al_2O_3$ catalyst showed slightly higher composition of surface carbon compared to the other two catalysts. Table 1 shows the IAg/IAl ratio which increased with increasing the silver loading from 0.01 to 0.07 and 0.11 for 1% Ag/η-$Al_2O_3$, 10% Ag/η-$Al_2O_3$ and 15% Ag/η-$Al_2O_3$, respectively.

It is worth noting that there is a probability of reduction of $Ag^{+1}$ under the reaction condition as the hydrogen in methanol is reductive, the reduction can be checked using XPS analysis (Ag MNN) for the fresh and the spent catalyst[41], which will be discussed later.

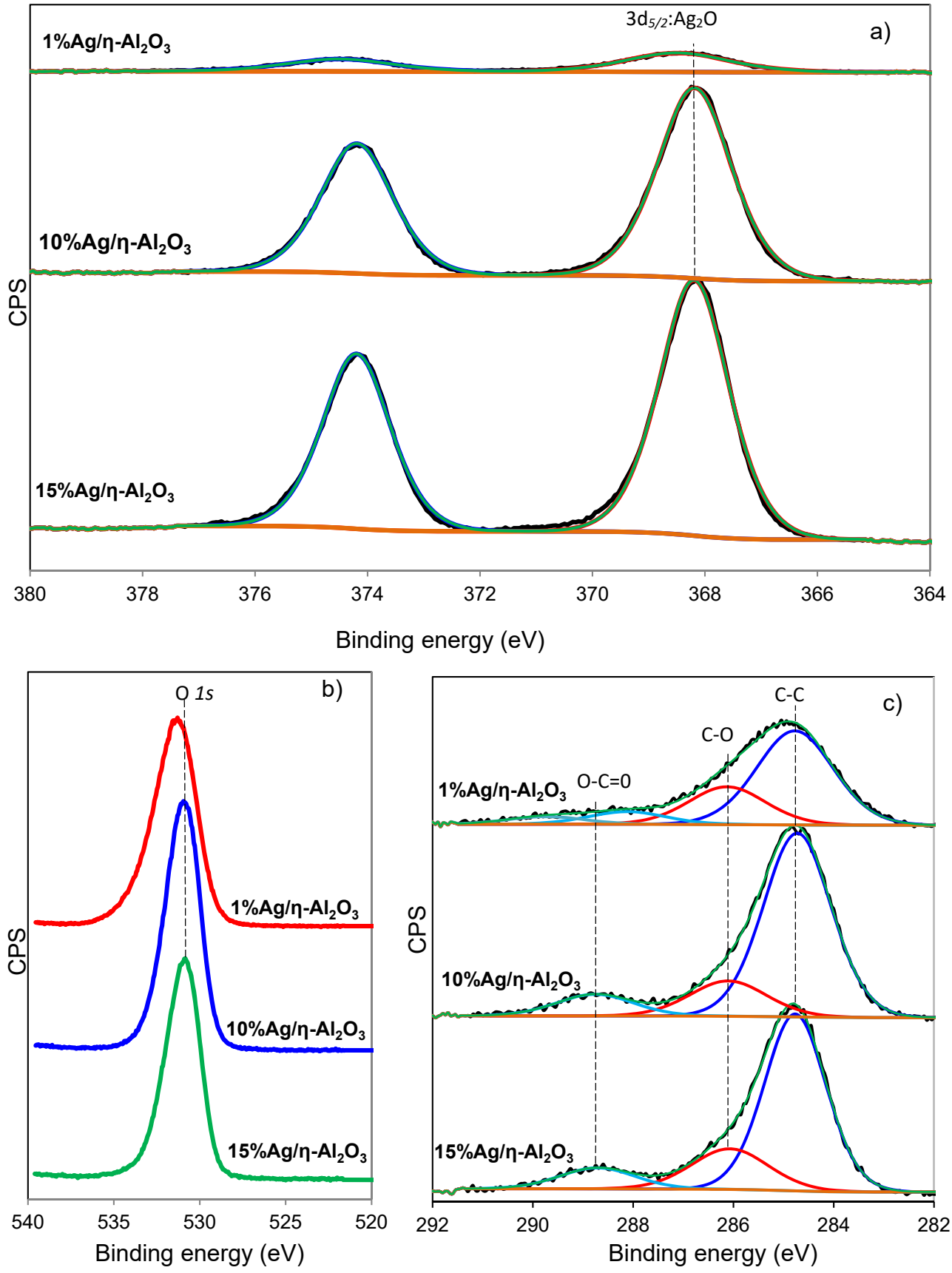


**Figure 6**: XPS of 1% Ag/η-$Al_2O_3$, 10% Ag/η-$Al_2O_3$ and 15% Ag/η-$Al_2O_3$ catalysts for a) Ag *3d*, b) O *1s* and c) Adventitious carbon C*1s*.

The surface hydrophobicity was measured according to the water contact angle (CA) as seen in Figure 7. The wettability of the catalyst surface, demonstrated by CA (θ) of a droplet of water, is assumed by Young's equation (Equation 15)

$$\cos\theta = \frac{\gamma_{SV} - \gamma_{SL}}{\gamma_{LV}} \quad (15)$$

Where, $\gamma_{SV}$, $\gamma_{SL}$ and $\gamma_{LV}$ stand for the interfacial surface tension of solid (S), liquid (L) and gas vapour (V. This equation is derived from the thermodynamic equilibrium of the free energy at the S-L-V interphase. The surface wettability is measured according to the CA and may be divided into four different categories; super-hydrophilic (θ <10º), hydrophilic (10 <θ <90º), hydrophobic (90 <θ <150º) and super-hydrophobic (θ >150º). It is well known that pure alumina catalyst is super-hydrophilic with CA approximately θ = 1.69º as seen in Figure 7 (a). The CA increased to 20.7º with 1% the Ag loading and then significantly increased to 50.7º at 10% Ag loading. However, with further increasing of the Ag loading, the CA slightly decreased to 39º, this is may be attributed to the Ag loading over the surface of the η-$Al_2O_3$ catalyst, i.e. at low Ag loading (1% Ag) there was a small number of Ag atoms covering the surface of η-$Al_2O_3$, while at 10% Ag loading there was a uniform distribution of the silver atoms that prevent the water adsorption. Further loading of silver (15% Ag) shows a formation of big clusters as seen from the SEM images in Figure 3. The enhanced hydrophobicity with Ag loadings confirmed by the FTIR spectra in Figure S4, where the OH band at 3300 $cm^{-1}$ disappeared at 10 and 15% Ag loading. Figure S4(b) shows the negative bands over pure η-$Al_2O_3$ and 10% Ag/η-$Al_2O_3$ catalysts at 50 °C due to the removal of surface hydroxyl groups. The negative band is due to the subtraction of the spectrum of the material before exposure to the reaction mixture. It is clear from Figure 5(b) that the negative band in case of 10% Ag/η-$Al_2O_3$ is less deep than that in case of pure η-$Al_2O_3$ due to the increased surface hydrophobicity as a result of silver addition. This comes in accordance with the observation from figure S4(a) which shows a complete disappearance of the band at 3500-3100 $cm^{-1}$ corresponding to surface hydroxyl by increase the Ag loading from 1 to 10 and 15%.

Figure 7 (d) shows the CA of the H-$Al_2O_3$ catalyst, θ = 170.6º i.e. super-hydrophobic materials. Schematic 1 depicts the superior enhancement in the hydrophobicity via the transformation of the super-hydrophilic η-$Al_2O_3$ (θ = 1.69º) into the super-hydrophobic alumina (θ = 170.6º) using the TEOOS reagent. Furthermore, the difference in the hydrophobicity is obvious as seen in video 1 of the water droplets on the surface of the super-hydrophilic and superhydrophobic alumina (η-$Al_2O_3$ and H-$Al_2O_3$) catalysts (using the yellow colour of ferric chloride for clarity) to illustrate the efficiency of the adopted approach used for the transformation of η-$Al_2O_3$ into H-$Al_2O_3$ . On the other hand, during this transformation, most of the Lewis acidic sites were removed as seen in Figure S5 compared with the η-$Al_2O_3$ catalyst.

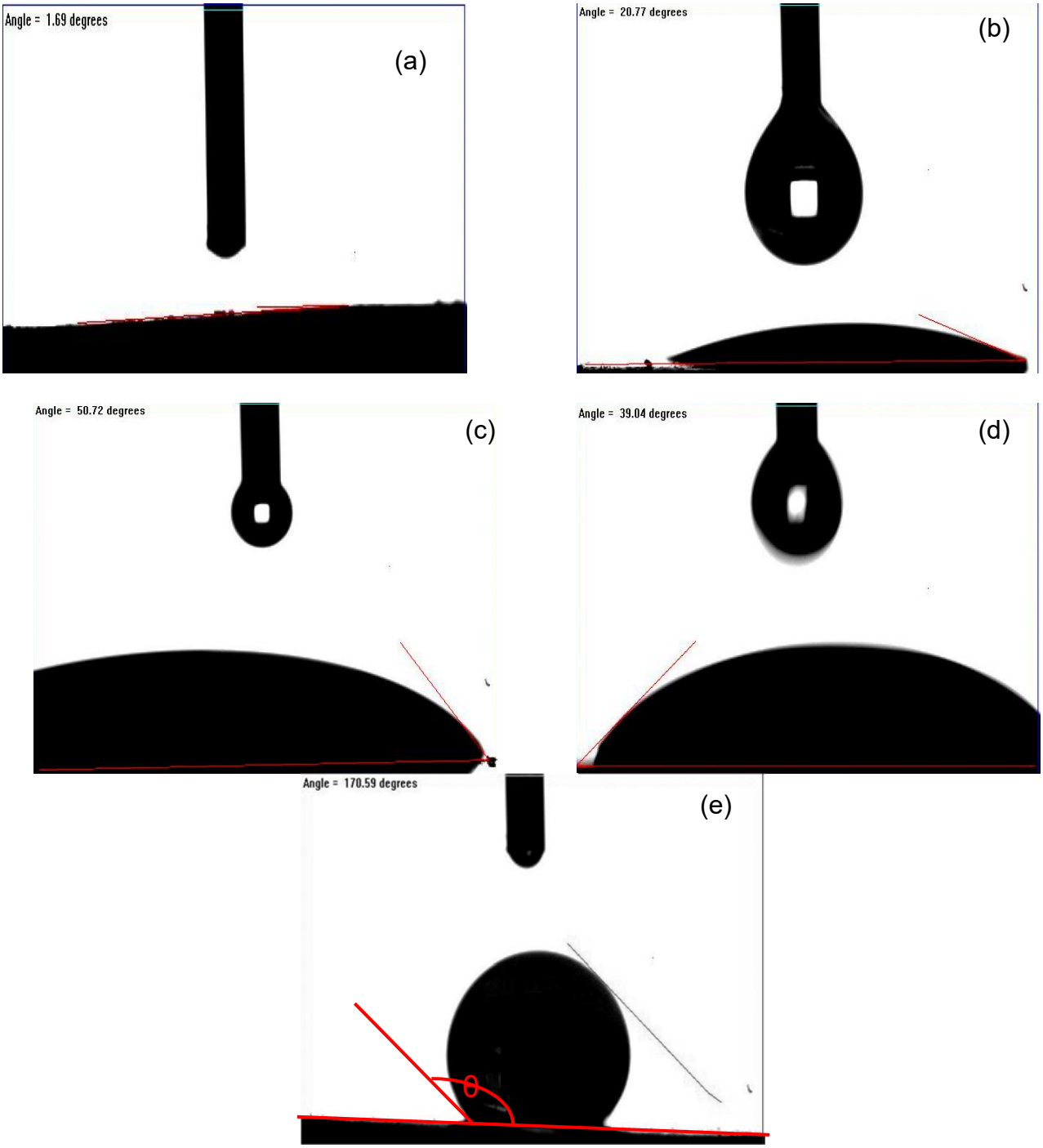


**Figure 7:** Comparison between hydrophobicity of catalyst surface of (a) pure η-$Al_2O_3$, (b) 1% Ag/η-$Al_2O_3$, (c) 10% Ag/η-$Al_2O_3$, (d) 15% Ag/η-$Al_2O_3$ and (e) H-$Al_2O_3$.

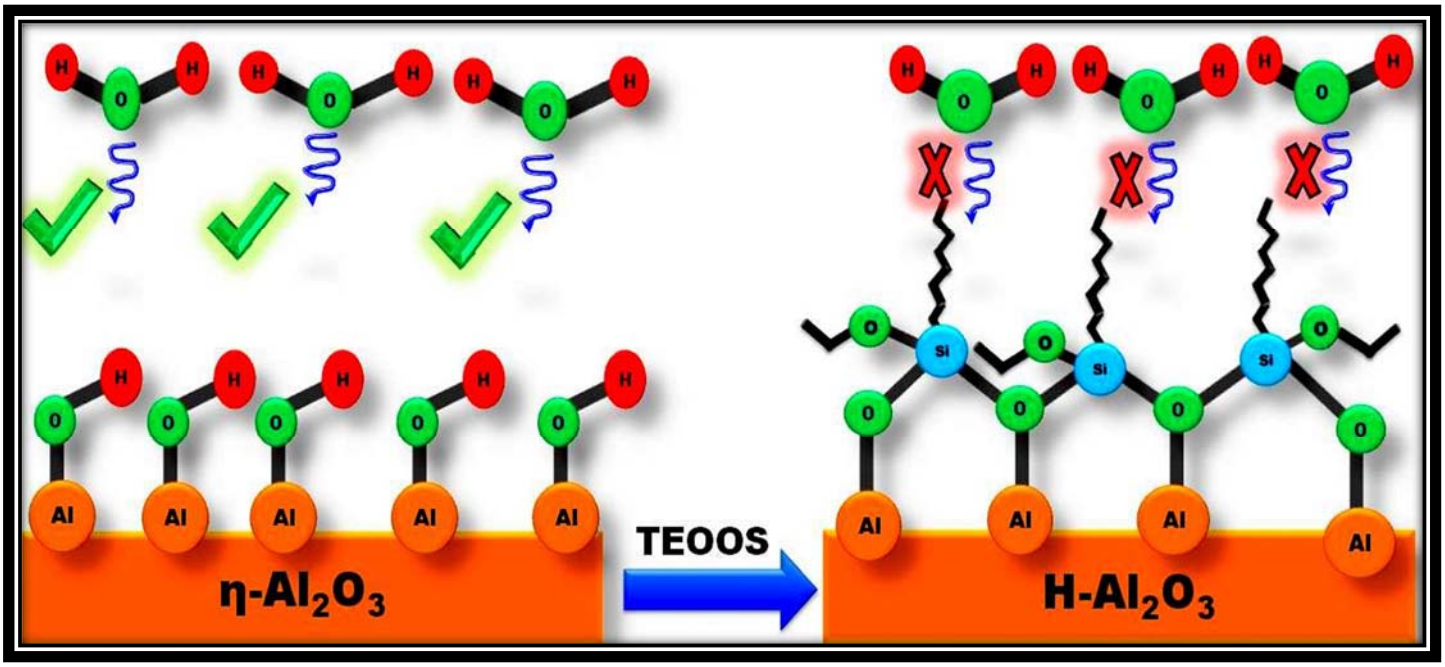


**Schematic 1:** Schematic representation of the super-hydrophilicity of η-$Al_2O_3$ and converting it into super-hydrophobic alumina support using triethoxyoctyl silane reagent (TEOOS).

Figure 8 (a) and (b) show transmission electron micrographs of the structure in bright field TEM and HAADF-STEM respectively with a selected area electron diffraction pattern inset. Figure 8 (c) and (d) show the silver atoms dispersion over the surface of the η-$Al_2O_3$ catalyst structure as well as high-resolution TEM (HRTEM) of a single Ag particle. It is clear from the SAED and HRTEM that the Ag particles are crystalline in nature and the TEM data shows that the size of these crystallites generally of < 5 nm in size. These particles distribute with relative uniformity across the surface of the alumina and these results are in agreement with the SEM results.

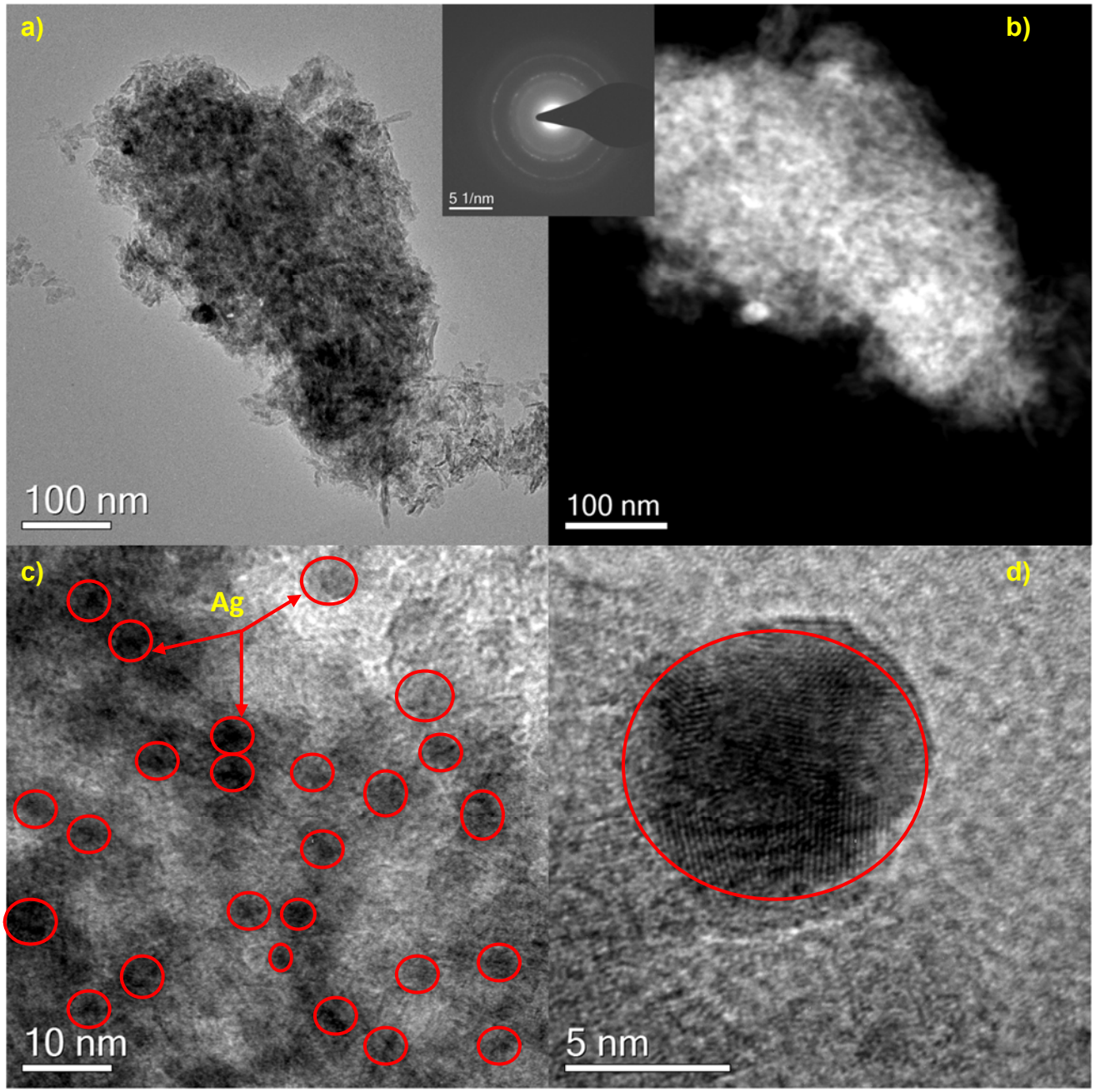


**Figure 8:** shows the TEM images (a) Bright field transmission electron micrograph of a 10% Ag/η-$Al_2O_3$ structure. (b) HAADF-STEM image of the same region. (c) Bright field TEM image showing the Ag particle distribution across the surface of the alumina. (d) HRTEM image of a single grain of Ag. The inset image is the SAED (Selected Area Electron Diffraction) pattern of a single 10% Ag/η-$Al_2O_3$ structure.

*4.2. Mechanism study of Ag loaded on* η-$Al_2O_3$ *using DRIFTS*

Figure 9 shows the DRIFT spectra of 10%Ag/$Al_2O_3$ sample obtained during the exposure to the reaction feed with a stepwise increase in the reaction temperature. The spectrum obtained for 10% Ag/η-$Al_2O_3$

seems to be similar, to some extent, to that of pure alumina with some differences. The spectrum obtained at 50°C is characterised by negative bands of surface hydroxyl groups (i.e. 3738, 3688 $cm^{-1}$) and bands corresponding to surface methoxy groups (2941, 2888, 2822, 2595 $cm^{-1}$) [9, 29-31]. In addition, the spectrum shows bands at 3260, 1800 and 1451 $cm^{-1}$ corresponding to hydrogen-bonded hydroxyl groups, adsorbed CO and carbonate–carboxylate species, respectively [29]. By increasing the temperature, a progressive decrease in the intensity of the bands at 3260, 2595, 1800 and 1451 $cm^{-1}$ is observed. In addition, bands at 3639, 1592, 1390 and 1374 $cm^{-1}$ started to appear starting from temperature 150 °C and then, their intensities increased with increasing temperature. The band at 3639 can be attributed to isolated hydroxyl groups which may be formed due to formate decomposition [29], which implies that decomposition of formate species produced OH groups. The bands at 1592, 1390 and 1374 $cm^{-1}$ are attributed to surface formate species. There are some differences between the spectra in the case of pure η-$Al_2O_3$ catalyst and that in the case of 10% Ag/η-$Al_2O_3$ catalyst. The removal of methoxy species over 10% Ag/η-$Al_2O_3$ seems to be faster and started at lower temperatures compared to that in the case of pure η-$Al_2O_3$. In addition, the removal of carbonate–carboxylate species was also faster over 10% Ag/η-$Al_2O_3$ surface and the band at 1451 $cm^{-1}$ was completely disappeared at 200°C. Furthermore, the bands corresponding to formate species appeared at a lower temperature in the case of 10% Ag/η-$Al_2O_3$ catalyst. Regarding the reaction mechanism, it is clear that the two DRIFTS spectra of pure (η-$Al_2O_3$) and silver modified alumina (10% Ag/η-$Al_2O_3$) are qualitatively similar which indicates that the reaction mechanism over the two catalysts is the same. From the DRIFTS results, the reaction seems to be faster over 10% Ag/η-$Al_2O_3$ catalyst compared to a pure η-$Al_2O_3$ sample which is one of the important factors responsible for the higher activity of 10% Ag/η-$Al_2O_3$ catalyst compared to pure η-$Al_2O_3$ sample. This enhancement in the reaction rate is probably due to the increase in surface hydrophobicity upon loading Ag on η-$Al_2O_3$. The increased hydrophobicity is expected to fasten the removal of the produced water from the catalyst surface which will eventually enhance the rate of reaction. This is in agreement with the FTIR-Pyridine results where both the two catalysts showed only Lewis acidic sites with 10% Ag/η-$Al_2O_3$ showed higher acidity

(Figure 5), implying that it is indeed more active than the pure alumina in MTD reaction as it is an acid catalysed reaction.

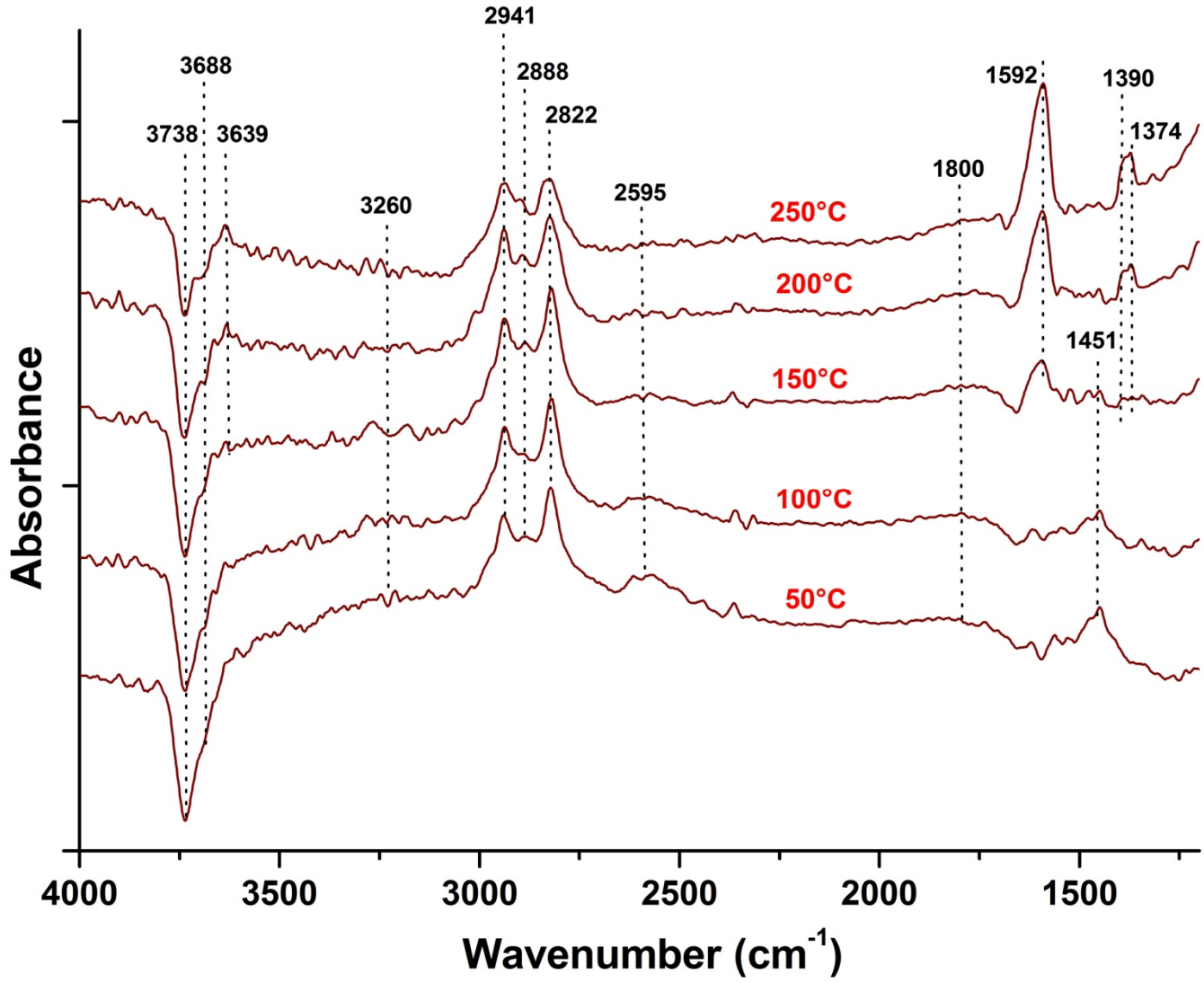


**Figure 9:** In-situ DRIFT spectra obtained over the 10% Ag/ η-$Al_2O_3$ catalyst during the interaction under reaction feed (20% MeOH+ He gas as an inert in the feed) at 50°C for 20 min followed by a stepwise heating to the indicated temperatures under the same reaction feed.

The TPR profiles of 1% Ag/η-$Al_2O_3$, 10% Ag/η-$Al_2O_3$ and 15% Ag/η-$Al_2O_3$ catalysts are shown in Figure 10. At low silver loading i.e. 1% wt. Ag, the catalyst showed three reduction peaks at 130, 193 and 565 °C, while at high Ag loadings (10 and 15 wt. %) these peaks were merged and appeared at approximately 120

and 200 °C. Interestingly, the pure η-$Al_2O_3$ catalyst showed no reduction peaks in the temperature range of -20 °C to 700 °C, so all the reduction peaks are characterised of the silver oxide species. The presence of three reduction peaks at 1% Ag/η-$Al_2O_3$ gives an indication of the presence of hardly reduced silver oxide species, especially the reduction peak at 565 °C. This is in line with the XPS results that showed Ag $3d_{5/2}$ and O*1s* peaks shift to lower binding energy with increasing silver loading i.e. the Ag loading facile the oxidation cycle [39]. Catalyst 10% Ag/ η-$Al_2O_3$ showed the lowest reduction peak at 119 °C indicating a facile reduction at 10 wt. % Ag, while at the highest Ag loading, this peak was shifted to a higher temperature (130 °C). By increasing the $Ag_2O$ species with the loading of Ag as confirmed from the XRD and XPS results, consequently, the reduction peaks (hydrogen consumption) increase with the silver loading as seen in Figure 10.

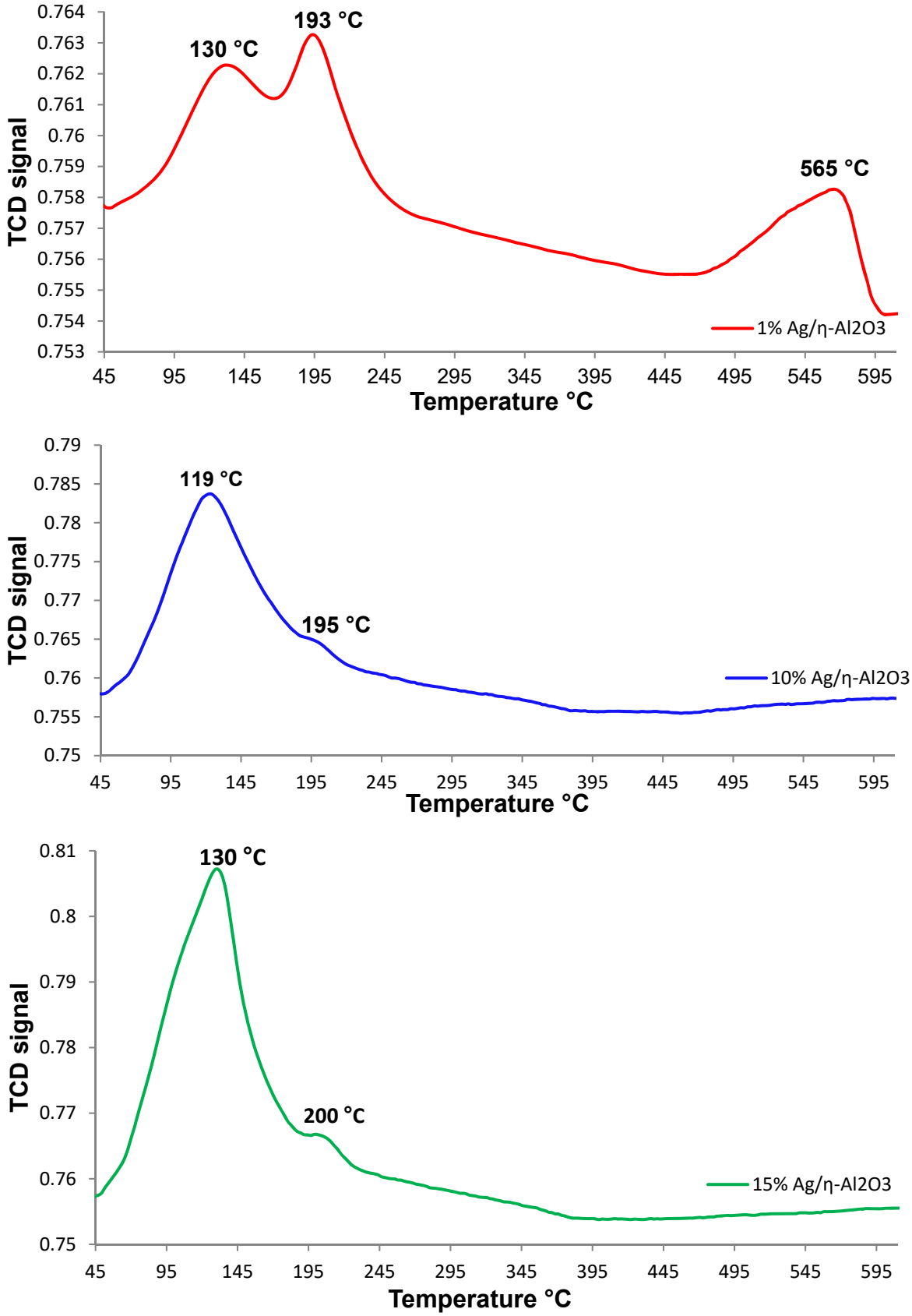


**Figure 10:** TPR profiles of 1% Ag/η-$Al_2O_3$, 10% Ag/η-$Al_2O_3$ and 15% Ag/η-$Al_2O_3$ catalysts.

*4.3 Catalyst activity of Ag modified alumina catalyst*

The effects of Ag loading on the η-$Al_2O_3$ catalyst for the MTD reaction carried out over the temperature range 180-300 °C along with the commercial γ-$Al_2O_3$ are shown in Figure (11). The catalytic activity was clearly increased with the increase in the Ag loading until it attained the maximum at an Ag loading of 10 wt. %, after which it slightly declined with further increase in the Ag loading (15 wt. %). For instance, at a high reaction temperature of 300 °C, the conversion of methanol over η-$Al_2O_3$ was 76.4 % which only increased by 8% i.e. to 84.5% upon adding 10 wt. % Ag and then decreased to 81.6 % over 15% Ag loading. Although there was a little enhancement in the catalytic activity at high temperature compared with the pure η-$Al_2O_3$, the conversion approached the equilibrium curve (dashed curve in Figure 11). Clearly, there was a significant increment in the catalytic performance at a low reaction temperature of 250 °C, where the conversion of methanol over η-$Al_2O_3$ was 18 % which increased more than twice to 39.5 % over 10%Ag/η-$Al_2O_3$ and then again slightly declined to 34% over 15% Ag loading. The same result can be observed from the DME reaction rate (not shown). Such differences are ascribed to differences in the surface acid strength as well as hydrophobicity properties. As discussed above for the 10% Ag loading, the hydrophobicity of the surface improved from superhydrophilic to hydrophilic (see Figure (7)) and stronger Lewis acidic sites were observed in the FTIR-Pyridine (Figure (5). To test the hypothesis that hydrophobicity is the only factor that affects the MTD reaction, a superhydrophobic alumina catalyst (H-$Al_2O_3$) was prepared and showed a CA of 170.6º implying a superhydrophobic surface, however, during the transformation of the superhydrophilic alumina into H-$Al_2O_3$, most of the acidic sites were removed and consequently the catalytic activity decreased as shown in Figure 11. To sum up, a balance between acidity and hydrophobicity is needed to achieve an optimum activity during the MTD reaction.

Heterogeneous catalyst deactivation can take place as a result of poisoning, vapour compound formation, fouling and vapour/solid or solid/solid reactions. The most common factors causing catalyst deactivation are poisoning, fouling or sintering. From the previous work, η-$Al_2O_3$ showed a high degree of stability

and had double the activity of the commercial γ-$Al_2O_3$ or 87% of the activity of commercial ZSM-5 (80) at 250 ˚C at WHSV of 12.1 $h^{-1}$ [7]. Raoof et al.[14] reported that water had the highest inhibition effect and dramatically deactivate the alumina catalyst by adding water in the reaction feed.

Figure 11 (b) shows the stability tests over a period of 60 h for the pure η-$Al_2O_3$ and the optimum modified silver catalyst (10% Ag/ η-$Al_2O_3$). Stability is one of the main requirements for such catalysts, while both catalysts were reasonably stable, the optimum catalyst in terms of both activity and stability appeared to be 10% Ag/ η-$Al_2O_3$ catalyst. In addition, the conversion of η-$Al_2O_3$ at 250 °C was clearly around 18 % while for 10% Ag/ η-$Al_2O_3$ catalyst, the conversion was approximately twice that with a value of 39 %.

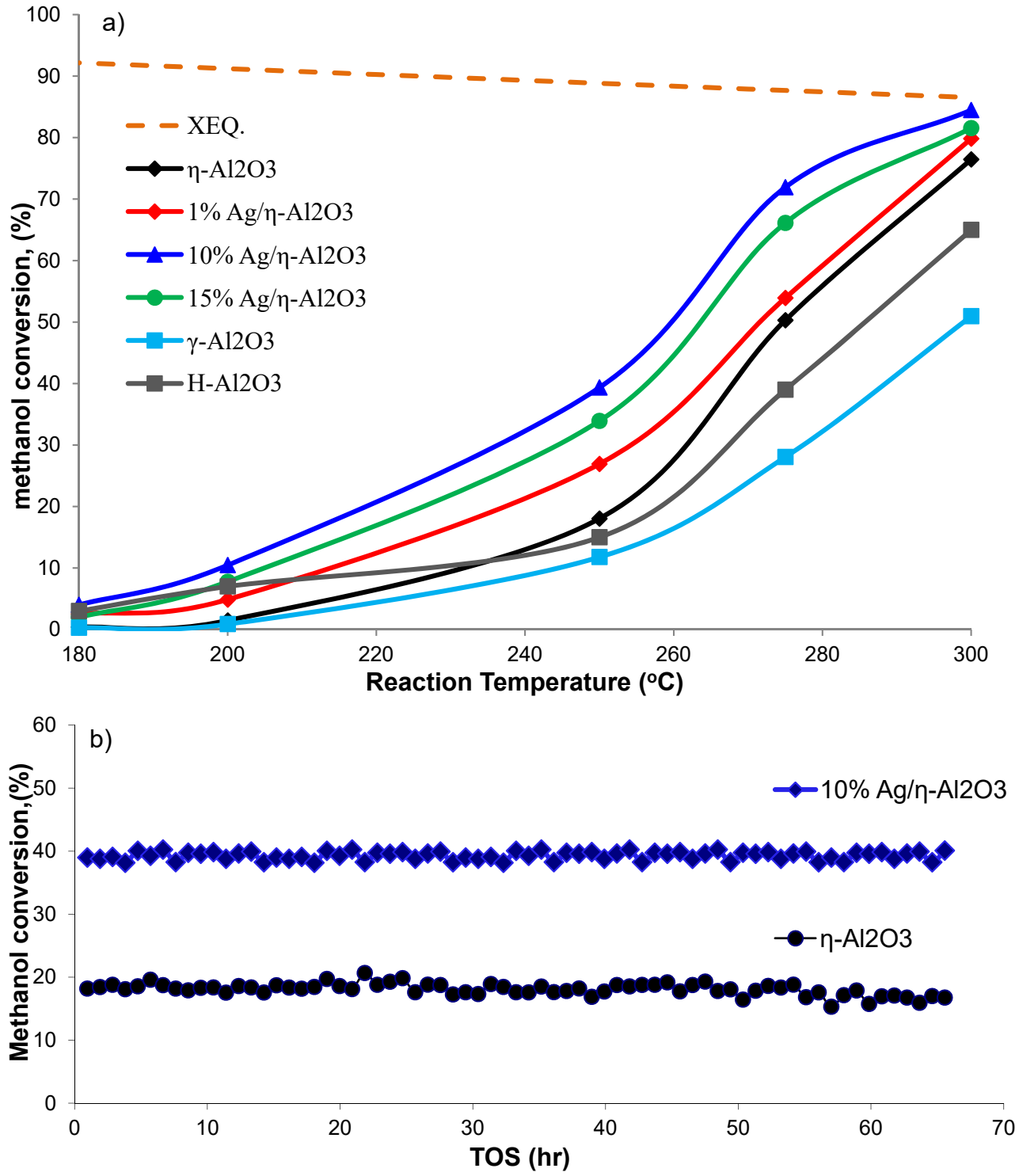


**Figure 11:** Catalytic activity profiles a) effect of reaction temperature on methanol dehydration to DME with different Ag loading along with the super-hydrophobic alumina (H-$Al_2O_3$), reaction condition; T= 180-300 °C; catalyst weight= 50 mg; He flow rate = 80 ml/min; WHSV: 48.4 $h^{-1}$. b) The time on stream test at 250 °C for the 10% Ag/η-$Al_2O_3$ and pure η-$Al_2O_3$ catalysts.

XPS was carried out to investigate the probability of reduction of $Ag^{+1}$ under the reaction conditions and determine silver oxidation state in the spent Ag modified catalysts. Ag $3d_{5/2}$ binding energies are very close for metallic silver and its oxides and generally, it is difficult to assign the oxidation state from Ag *3d* alone. However, the auger peak Ag MNN allows reliable distinguishing of Ag(0) and Ag(+1) [41]. In the subsequent study, Ag *3d* and Ag MNN Auger structure region were acquired on the fresh and spent 10% Ag/η-$Al_2O_3$ and 15% Ag/η-$Al_2O_3$ catalysts keeping acquisition times short and consistent to minimise beam effects. Ag $3d_{5/2}$ binding energies for the fresh and spent catalysts show only 0.1 - 0.2 eV shift (Figure S6). However, the auger Ag MNN peaks in Figure 12 show significant differences for the fresh and spent catalysts. The 10% Ag/η-$Al_2O_3$ fresh catalyst shows two peaks at kinetic energies(KE) approx. 348.5 eV and 354.9 eV. The modified Auger parameter [42] calculated at 716.7 and 723.1 eV is consistent with $Ag^{+1}$ species [41]. However, Ag MNN structure of the 10% Ag/η-$Al_2O_3$ spent catalyst shows three peaks. The peaks at 352 and 357.8 eV gives auger parameters at 720.1 eV and 725.9 eV and are consistent with metallic Ag [41]. However, the third peak at 348.5 eV remains in the spent catalyst indicative of the presence of silver oxide and thus clearly suggesting that not all $Ag^{+1}$ is reduced to silver, and that both Ag and $Ag^{+1}$ coexist. The 15% Ag/η-$Al_2O_3$ spent catalyst also show the same peak structure (Figure 12 (d)). It is likely that $Ag^{+1}$ at only some sites are more prone to reduction, or those on the surface may reduce easily in the feed reducing environment. As the 10% Ag/η-$Al_2O_3$ catalyst was stable in the time on stream test over a period of 60 h, this suggests that presence of Ag enhance the surface hydrophobicity of alumina regardless of its oxidation state whether it was (0) or (+1). Moreover, it was reported that Ag (0) can promote the surface hydrophobicity [18].

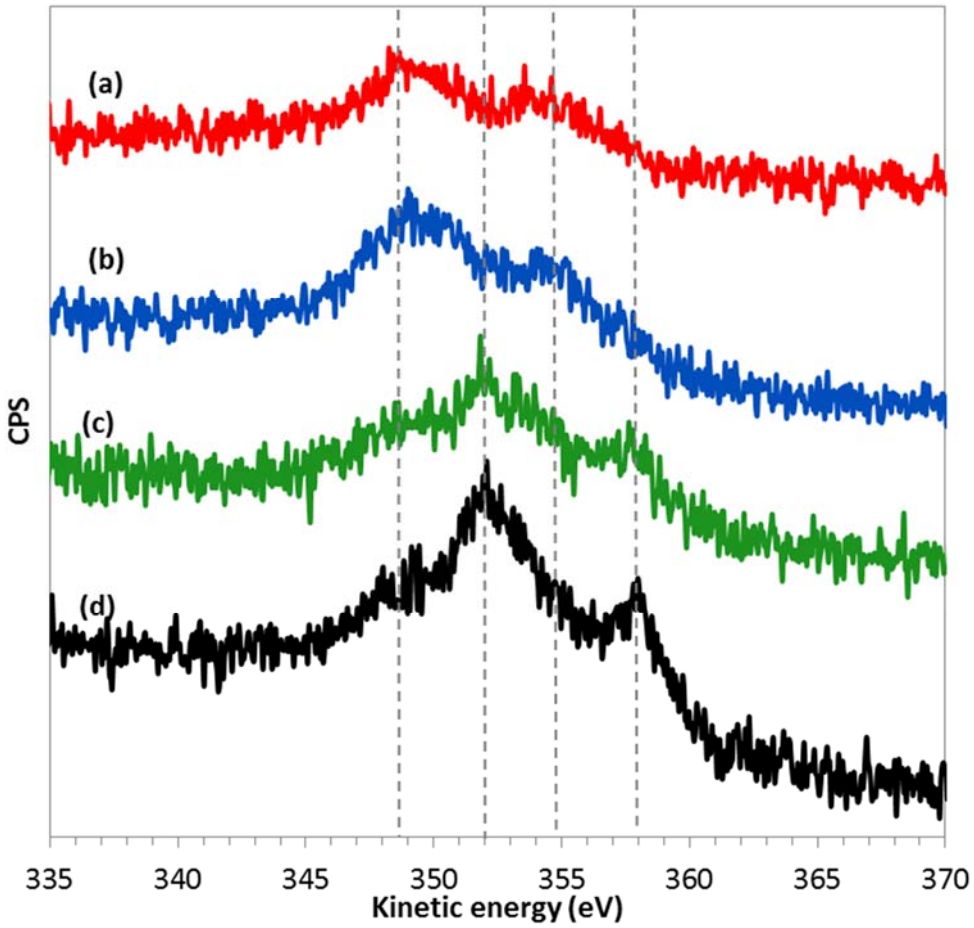


**Figure 12**: Ag MNN Auger structure region for (a) fresh 10% Ag/η-$Al_2O_3$ (b) fresh 15% Ag/η-$Al_2O_3$ (c) spent 10% Ag/η-$Al_2O_3$ and (d) spent 15% Ag/η-$Al_2O_3$ respectively.

## 5. Conclusions

In-situ DRIFTS were studied to investigate the reaction mechanism of methanol dehydration over the pure η-$Al_2O_3$ catalyst. Moreover, the effect of silver loading on the catalytic performance of η-$Al_2O_3$ was examined in a fixed bed reactor under the reaction conditions where the temperature ranged from 180-300 °C with a WHSV= 48.4 $h^{-1}$. The addition of silver to the support improved the catalytic activity and herein, the optimum catalyst was 10% Ag/η-$Al_2O_3$. The Ag loadings clearly resulted in an improvement in the Lewis acidity and in the secondary improvement of the bulk surface properties by changing the surface from superhydrophilic to hydrophilic at 10% Ag loading with an increase in the CA from 1.6 to 50.7 º for pure η-$Al_2O_3$ and 10% Ag/η-$Al_2O_3$, respectively. Furthermore, 10% Ag/η-$Al_2O_3$ catalyst exhibited a high degree of stability under steady-state conditions and this is attributed to the enhancement in both surface Lewis acidity and hydrophobicity. To test the hypothesis that hydrophobicity is the only factor that affects the MTD reaction, a superhydrophobic alumina catalyst (H-$Al_2O_3$) was prepared and showed a CA of 170.6º, however, during the transformation of the superhydrophilic alumina into H-$Al_2O_3$, most of the acidic sites were removed and consequently the catalytic activity decreased compared with the pure η-$Al_2O_3$. To summarise, a balance between acidity and hydrophobicity is needed to achieve an optimum activity during the MTD reaction which was achieved herein in the 10%Ag/η-$Al_2O_3$ catalyst.

**Supporting Information:** Nitrogen adsorption-desorption isotherms, SEM images, EDX data, FT-IR and In-situ DRIFT, XPS

**Competing financial interests:** The authors declare no competing financial interests.

**Acknowledgements:** The authors would like to acknowledge the support given to AO from South Valley University in Egypt and all the support given by the School of Chemistry and Chemical Engineering, Queen's University Belfast.

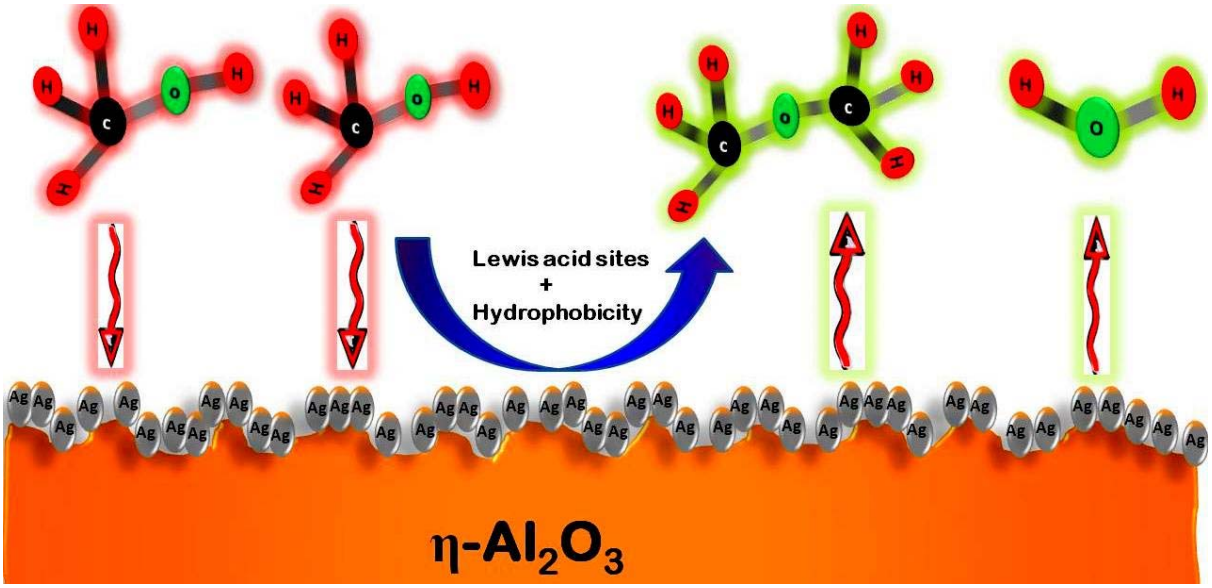


TOC Graphic

## 6. References

1. Khoshbin, R.; Haghighi, M., Direct Conversion of Syngas to Dimethyl Ether as a Green Fuel over Ultrasound-Assisted Synthesized Cuo-Zno-$Al_2o_3$/Hzsm-5 Nanocatalyst: Effect of Active Phase Ratio on Physicochemical and Catalytic Properties at Different Process Conditions. *Catal. Sci. Technol.* **2014**, *4*, 1779-1792.
2. Figoli, N. S.; Hillar, S. A.; Parera, J. M., Poisoning and Nature of Alumina Surface in the Dehydration of Methanol. *J. Catal.* **1971**, *20*, 230-237.
3. Asthana, S.; Samanta, C.; Bhaumik, A.; Banerjee, B.; Voolapalli, R. K.; Saha, B., Direct Synthesis of Dimethyl Ether from Syngas over Cu-Based Catalysts: Enhanced Selectivity in the Presence of Mgo. *J. Catal.* **2016**, *334*, 89-101.
4. Cai, M.; Palcic, A.; Subramanian, V.; Moldovan, S.; Ersen, O.; Valtchev, V.; Ordomsky, V. V.; Khodakov, A. Y., Direct Dimethyl Ether Synthesis from Syngas on Copper–Zeolite Hybrid Catalysts with a Wide Range of Zeolite Particle Sizes. *J. Catal.* **2016**, *338*, 227-238.
5. Osman, A. I.; Abu-Dahrieh, J. K.; McLaren, M.; Laffir, F.; Nockemann, P.; Rooney, D., A Facile Green Synthetic Route for the Preparation of Highly Active Γ-$Al_2o_3$ from Aluminum Foil Waste. *Sci. Rep.* **2017**, *7*, 3593.
6. Royaee, S. J.; Falamaki, C.; Sohrabi, M.; Ashraf Talesh, S. S., A New Langmuir–Hinshelwood Mechanism for the Methanol to Dimethylether Dehydration Reaction over Clinoptilolite-Zeolite Catalyst. Appl. Catal., *A.* **2008**, *338*, 114-120.
7. Osman, A. I.; Abu-Dahrieh, J. K.; Rooney, D. W.; Halawy, S. A.; Mohamed, M. A.; Abdelkader, A., Effect of Precursor on the Performance of Alumina for the Dehydration of Methanol to Dimethyl Ether. Appl. Catal., *B.* **2012**, *127*, 307-315.
8. Hosseininejad, S.; Afacan, A.; Hayes, R. E., Catalytic and Kinetic Study of Methanol Dehydration to Dimethyl Ether. *Chem. Eng. Res. and Des.***2012**, *90*, 825-833.
9. Akarmazyan, S. S.; Panagiotopoulou, P.; Kambolis, A.; Papadopoulou, C.; Kondarides, D. I., Methanol Dehydration to Dimethylether over $Al_2O_3$ Catalysts. Appl. Catal., *B.* **2014**, *145*, 136-148.
10. Camposeco, R.; Castillo, S.; Mejia-Centeno, I.; Navarrete, J.; Rodriguez-Gonzalez, V., Behavior of Lewis and Brönsted Surface Acidity Featured by Ag, Au, Ce, La, Fe, Mn, Pd, Pt, V and W Decorated on Protonated Titanate Nanotubes. *Microporous Mesoporous. Mater.* **2016**, *236*, 235-243.
11. Gora-Marek, K.; Tarach, K. A.; Piwowarska, Z.; Laniecki, M.; Chmielarz, L., Ag-Loaded Zeolites Y and Usy as Catalysts for Selective Ammonia Oxidation. *Catal. Sci. Technol.* **2016**, *6*, 1651-1660.
12. Alamolhoda, S.; Kazemeini, M.; Zaherian, A.; Zakerinasab, M. R., Reaction Kinetics Determination and Neural Networks Modeling of Methanol Dehydration over Nano γ-$Al_2O_3$ Catalyst. *J. Ind. Eng. Chem.* **2012,** 18,(6), 2059-2068.
13. Xu, M. T.; Lunsford, J. H.; Goodman, D. W.; Bhattacharyya, A., Synthesis of Dimethyl Ether (DME) from Methanol over Solid-Acid Catalysts. Appl. Catal., *A.* **1997**, *149*, 289-301.
14. Lertjiamratn, K.; Praserthdam, P.; Arai, M.; Panpranot, J., Modification of Acid Properties and Catalytic Properties of $AlPO_4$ by Hydrothermal Pretreatment for Methanol Dehydration to Dimethyl Ether. Appl. Catal., *A.* **2010**, *378*, 119-123.
15. Raoof, F.; Taghizadeh, M.; Eliassi, A.; Yaripour, F., Effects of Temperature and Feed Composition on Catalytic Dehydration of Methanol to Dimethyl Ether over Alumina. *Fuel* **2008**, *87*, 2967-2971.
16. Kim, S. D.; Baek, S. C.; Lee, Y.-J.; Jun, K.-W.; Kim, M. J.; Yoo, I. S., Effect of Alumina Content on Catalytic Performance of Modified ZSM-5 for Dehydration of Crude Methanol to Dimethyl Ether. Appl. Catal., *A.* **2006**, *309*, 139-143.
17. Zhao, N.; Shi, F.; Wang, Z.; Zhang, X., Combining Layer-by-Layer Assembly with Electrodeposition of Silver Aggregates for Fabricating Superhydrophobic Surfaces. *Langmuir* **2005**, *21*, 4713-4716.
18. Feng, X.; Shi, Y.; Wang, Y.; Yue, G.; Yang, W., Preparation of Superhydrophobic Silver Nano Coatings with Feather-Like Structures by Electroless Galvanic Deposition. *Chin. Sci. Bull.* **2013**, *58*, 1887-1891.
19. Li, Z.; Sun, Z.; Duan, Z.; Li, R.; Yang, Y.; Wang, J.; Lv, X.; Qi, W.; Wang, H., Super-Hydrophobic Silver-Doped $TiO_2$ @ Polycarbonate Coatings Created on Various Material Substrates with Visible-Light Photocatalysis for Self-Cleaning Contaminant Degradation. *Sci. Rep.* **2017**, *7*, 42932.
20. Wu, M.; Ma, B.; Pan, T.; Chen, S.; Sun, J., Silver-Nanoparticle-Colored Cotton Fabrics with Tunable Colors and Durable Antibacterial and Self-Healing Superhydrophobic Properties. *Adv. Funct. Mater.* **2016**, *26*, 569-576.

21. Osman, A. I.; Abu-Dahrieh, J. K.; Rooney, D. W.; Thompson, J.; Halawy, S. A.; Mohamed, M. A., Surface Hydrophobicity and Acidity Effect on Alumina Catalyst in Catalytic Methanol Dehydration Reaction. *J. Chem. Technol. Biotechnol.* **2017**, doi:10.1002/jctb.5371.

22. Jo, H.; Jung, H.; Park, J.; Jung, K.-D., Surface Modification of H–$Al_2O_3$ by $SiO_2$ Impregnation to Enhance Methanol Dehydration Activity. *Bull. Korean. Chem. Soc.* **2017**, *38*, 307-312.
23. Azis, M. M.; Harelind, H.; Creaser, D., On the Role of $H_2$ to modify Surface NOx Species over Ag-$Al_2O_3$ as Lean Nox Reduction Catalyst: TPD and DRIFT Studies. *Catal. Sci. Technol.* **2015**, *5*, 296-309.
24. Ralphs, K.; D'Agostino, C.; Burch, R.; Chansai, S.; Gladden, L. F.; Hardacre, C.; James, S. L.; Mitchell, J.; Taylor, S. F. R., Assessing the Surface Modifications Following the Mechanochemical Preparation of a Ag/$Al_2O_3$ Selective Catalytic Reduction Catalyst. *Catal. Sci. Technol.* **2014**, *4*, 531-539.
25. Tamm, S.; Vallim, N.; Skoglundh, M.; Olsson, L., The Influence of Hydrogen on the Stability of Nitrates During $H_2$-Assisted SCR over Ag/$Al_2o_3$ Catalysts – a Drift Study. *J. Catal.* **2013**, *307*, 153-161.
26. Kim, P. S.; Kim, M. K.; Cho, B. K.; Nam, I.-S.; Oh, S. H., Effect of $H_2$ on Denox Performance of HC-SCR over Ag/$Al_2O_3$: Morphological, Chemical, and Kinetic Changes. *J. Catal.* **2013**, *301*, 65-76.
27. Zhang, L.; He, H., Mechanism of Selective Catalytic Oxidation of Ammonia to Nitrogen over Ag/$Al_2O_3$. *J. Catal.* **2009**, *268*, 18-25.
28. Abu-Dahrieh, J.; Rooney, D.; Goguet, A.; Saih, Y., Activity and Deactivation Studies for Direct Dimethyl Ether Synthesis Using Cuo-Zno-$Al_2o_3$ with NH4ZSM-5, HZSM-5 or γ-$Al_2O_3$. *Chem. Eng. J.* **2012**, *203*, 201-211.
29. Cao, C.; Hohn, K. L., Study of Reaction Intermediates of Methanol Decomposition and Catalytic Partial Oxidation on Pt/$Al_2o_3$. Appl. Catal., *A.* **2009**, *354*, 26-32.
30. Jacobs, G.; Davis, B. H., In Situ Drifts Investigation of the Steam Reforming of Methanol over Pt/Ceria. Appl. Catal., *A.* **2005**, *285*, 43-49.
31. McInroy, A. R.; Lundie, D. T.; Winfield, J. M.; Dudman, C. C.; Jones, P.; Parker, S. F.; Taylor, J. W.; Lennon, D., An Infrared and Inelastic Neutron Scattering Spectroscopic Investigation on the Interaction of Alumina and Methanol. *Phys. Chem. Chem. Phys.* **2005**, *7*, 3093-3101.
32. Perrichon, V.; Pijolat, M.; Primet, M., Surface Species Involved During the Hydrogenation of CO or $CO_2$ on Iron-Alumina Catalysts. *J. Mol. Catal.* **1984**, *25*, 207-217.
33. Appel, L. G.; Eon, J. G.; Schmal, M., The Co2–$CeO_2$ Interaction and Its Role in the $CeO_2$ Reactivity. *Catal. Lett.* **1998**, *56*, 199-202.
34. Lima, S. H.; Forrester, A. M. S.; Amparo Palacio, L.; Faro Jr, A. C., Niobia-Alumina as Methanol Dehydration Component in Mixed Catalyst Systems for Dimethyl Ether Production from Syngas. Appl. Catal., *A.* **2014**, *488*, 19-27.
35. Yuan, L.; Guo, S.; Li, Z.; Cui, H.; Dong, H.; Zhao, L.; Wang, J., Ring Opening of Decalin over Bifunctional Ni-W Carbide/$Al_2O_3$-Usy Catalysts and Monofunctional Acid Ni-W Oxide/$Al_2O_3$-Usy. *RSC Adv.* **2017**, *7*, 9446-9455.
36. Gannoruwa, A.; Ariyasinghe, B.; Bandara, J., The Mechanism and Material Aspects of a Novel $Ag_2O/TiO_2$ Photocatalyst Active in Infrared Radiation for Water Splitting. *Catal. Sci. Technol.* **2016**, *6*, 479-487.
37. Niemantsverdriet, J. W., Spec. in Cat. : An Introduction. 2nd ed. ed.; Wiley-VCH: Weinheim ;, 2000.
38. Nie, L. H.; Meng, A. Y.; Yu, J. G.; Jaroniec, M., Hierarchically Macro-Mesoporous Pt/gamma-$Al_2O_3$ Composite Microspheres for Efficient Formaldehyde Oxidation at Room Temperature. *Sci Rep-Uk* **2013**, *3*, 3215.
39. Strohmeier, B. R., Gamma-Alumina (γ-$Al_2O_3$) by XPS. *Surf. Sci. Spectra.* **1994**, *3*, 135-140.
40. Hu, J.; Zhong, Z. X.; Zhang, F.; Xing, W. H.; Low, Z. X.; Fan, Y. Q., Coating of Zno Nanoparticles onto the Inner Pore Channel Surface of Sic Foam to Fabricate a Novel Antibacterial Air Filter Material. *Ceram. Int.* **2015**, *41*, 7080-7090.
41. Ferraria, A. M.; Carapeto, A. P.; Botelho do Rego, A. M., X-Ray Photoelectron Spectroscopy: Silver Salts Revisited. *Vacuum* **2012**, *86*, 1988-1991.

42. Briggs D, Grant JT, editors. Surface analysis by auger and X-ray photoelectron spectroscopy. Chichester: IM Publications; 2003.